Journal of Animal Ecology

Disentangling serology to elucidate henipa- and filovirus transmission in Madagascar fruit bats

Journal:	*Journal of Animal Ecology*
Manuscript ID	JAE-2018-00609.R1
Manuscript Type:	Research Article
Date Submitted by the Author:	n/a
Complete List of Authors:	Brook, Cara E.; University of California Berkeley, Integrative Biology Ranaivoson, Hafaliana; Institut Pasteur de Madagascar, Virology Unit Broder, Christopher; Uniformed Services University of the Health Sciences, Department of Microbiology and Immunology Cunningham, Andrew; Zoological Society of London, Reader & Head of Wildlife Epidemiology Heraud, Jean-Michel; Institut Pasteur de Madagascar, Virology Unit Peel, Alison; Griffith University, Gibson, Louise; Zoological Society of London, Reader & Head of Wildlife Epidemiology Wood, James; Cambridge Infectious Diseases Consortium, Metcalf , Jessica ; Princeton University, Department of Ecology and Evolutionary Biology Dobson, Andy; Princeton University,
Key-words:	age-seroprevalence, filovirus, flying fox, force of infection, fruit bat, henipavirus, Madagascar, zoonosis

Disentangling serology to elucidate henipa- and filovirus transmission in Madagascar fruit bats

Cara E. Brook[1†], Hafaliana C. Ranaivoson[2,3], Christopher C. Broder[4], Andrew A. Cunningham[5], Jean-Michel Héraud[2], Alison J. Peel[6], Louise Gibson[5], James L.N. Wood[7], C. Jessica Metcalf [1]*, Andrew P. Dobson[1]*

[1]Department of Ecology & Evolutionary Biology, Princeton University, Princeton, NJ, USA.

[2] Virology Unit, Institut Pasteur de Madagascar, Antananarivo, Madagascar.

[3]Department of Animal Biology, University of Antananarivo, Antananarivo, Madagascar.

[4]Department of Microbiology and Immunology, Uniformed Services University, Bethesda, MD, USA.

[5]Institute of Zoology, Zoological Society of London, London, UK.

[6]Environmental Futures Research Institute, Griffith University, Nathan, QLD, Australia.

[7]Department of Veterinary Medicine, University of Cambridge, Cambridge, UK.

[†] *Corresponding author at:*

Department of Integrative Biology, UC Berkeley, Berkeley, CA USA;

email: cbrook@berkeley.edu

**These senior authors contributed equally to this work.*

Abstract

1. Bats are reservoirs for emerging human pathogens, including Hendra and Nipah henipaviruses and Ebola and Marburg filoviruses. These viruses demonstrate predictable patterns in seasonality and age structure across multiple systems; previous work suggests that they may circulate in Madagascar's endemic fruit bats, which are widely consumed as human food.

2. We aimed to (a) document the extent of henipa- and filovirus exposure among Malagasy fruit bats, (b) explore seasonality in seroprevalence and serostatus in these bat populations, and (c) compare mechanistic hypotheses for possible transmission dynamics underlying these data.

3. To this end, we amassed and analyzed a unique dataset documenting longitudinal serological henipa- and filovirus dynamics in three Madagascar fruit bat species.

4. We uncovered serological evidence of exposure to Hendra/Nipah-related henipaviruses in *Eidolon dupreanum, Pteropus rufus,* and *Rousettus madagascariensis,* to Cedar-related henipaviruses in *E. dupreanum* and *R. madagascariensis* and to Ebola-related filoviruses in *P. rufus* and *R. madagascariensis.* We demonstrated significant seasonality in population-level seroprevalence and individual serostatus for multiple viruses across these species, linked to the female reproductive calendar. An age-structured subset of the data highlighted evidence of waning maternal antibodies in neonates, increasing seroprevalence in young, and decreasing seroprevalence late in life. Comparison of mechanistic epidemiological models fit to these data offered support for transmission hypotheses permitting waning antibodies but retained immunity in adult-age bats.

5. Our findings suggest that bats may seasonally modulate mechanisms of pathogen control, with consequences for population-level transmission. Additionally, we narrow the field of candidate transmission hypotheses by which bats are presumed to host and transmit potentially zoonotic viruses globally.

Keywords: age-seroprevalence, filovirus, flying fox, force of infection, fruit bat, henipavirus, Madagascar, zoonosis

Introduction

Bats have received much attention in recent years for their roles as reservoirs for several virulent, emerging human pathogens, including Hendra and Nipah henipaviruses, Ebola and Marburg filoviruses, and SARS coronavirus (Calisher, Childs, Field, Holmes, & Schountz, 2006; Munster et al., 2016; Olival et al., 2017). Despite their infamy, bat viruses are not well understood. Elucidation of viral transmission dynamics in bat hosts will be essential to preventing future cross-species emergence by facilitating predictions of viral shedding pulses thought to underpin spillover (Amman et al., 2012) and by highlighting intervention opportunities in enzootic disease cycles.

Serology often represents the most readily attainable empirical information for wildlife diseases; methods have been developed to infer dynamics underlying patterns of age-structured seroprevalence for immunizing infections and prevalence for persistent infections (Brook et al., 2017; Farrington, 1990; Grenfell & Anderson, 1985; Griffiths, 1974; Heisey, Joly, & Messier, 2006; Hens et al., 2010; Long et al., 2010; Muench, 1959; Pomeroy et al., 2015). Numerous studies have reported serological evidence of bat exposure to henipa- and filoviruses across the Old World (Epstein et al., 2013, 2008, Hayman et al., 2010, 2008; Iehlé et al., 2007; Leroy et al., 2005; Ogawa et al., 2015; Peel et al., 2012; Plowright et al., 2008; Taniguchi et al., 1999; Yuan et al., 2012), though only a few have attempted to use mechanistic models to infer transmission dynamics from serological data for any bat virus (*e.g.* for rabies: Blackwood, Streicker, Altizer, & Rohani, 2013; for henipavirus: Peel et al., 2018). The paucity of attempts to model such data may be attributable to the idiosyncratic

landscape of chiropteran antibody responses. Experimental challenge trials with various bat species have demonstrated seroconversion post-inoculation with Hendra (Williamson et al., 1998) and Nipah (Middleton et al., 2007) henipaviruses and with Marburg (Amman et al., 2014; Paweska et al., 2015; Paweska et al., 2012; Schuh et al., 2017), Ebola, and Sudan filoviruses (Jones et al., 2015; Paweska et al., 2016), though many studies (*e.g.* Halpin et al., 2011) report idiosyncratic antibody dynamics of seroconversion without demonstrable viral replication. Only a few studies have followed immunized bats for longer time horizons: in Marburg-immunized *Rousettus aegyptiacus*, antibody titers wane post-inoculation and primary seroconversion, but subsequently re-challenged seronegative bats nonetheless remain protected from reinfection and primed to remount rapid antibody responses (Paweska et al., 2015; Schuh et al., 2017). The underlying immunological mechanisms for these responses remain unclear, but at least two pteropodid species were recently shown to maintain a constitutively expressed interferon complex (Zhou et al., 2016), offering an innate, non-antibody-mediated pathway for viral control.

The island of Madagascar is home to three endemic Old World Fruit Bat species, *Pteropus rufus, Eidolon dupreanum,* and *Rousettus madagascariensis,* with respective Asian (Almeida, Giannini, Simmons, & Helgen, 2014), African (Shi et al., 2014), and pan-Indian Ocean (Goodman, Chan, Nowak, & Yoder, 2010) origins. All three species are widely consumed across the island as bushmeat (Golden, Bonds, Brashares, Rasolofoniaina, & Kremen, 2014; Jenkins et al., 2011; Jenkins & Racey, 2008), offering abundant opportunities for zoonotic transmission. Previous work reports serological evidence of Hendra- and Nipah-related henipavirus spp. in *P. rufus* and *E. dupreanum* bats, as well as Tioman spp. virus in *R. madagascariensis* (Iehlé et al., 2007). To date, no filoviruses have been investigated in any Malagasy bat, although one early serosurvey of human communities in Madagascar

73 highlights seropositivity to Ebola-related filoviruses (but not Marburg) in several localities
74 across the island (Mathiot, Fontenille, Georges, & Coulanges, 1989). Recent modeling work
75 has classed Madagascar within the 'zoonotic niche' for both Ebola (Pigott et al., 2014) and
76 Marburg virus disease (Pigott et al., 2015). These intriguing preliminary findings, combined
77 with the extreme virulence and heavy public health cost of known bat-to-human henipa- and
78 filovirus emergence events, motivated our study. We aimed to (1) document the extent of
79 henipa- and filovirus spp. exposure among endemic Malagasy fruit bats, (2) explore patterns
80 of seasonality in seroprevalence and serostatus in these populations, and (3) compare
81 mechanistic hypotheses for possible transmission dynamics underlying these data.
82

83 **Materials and Methods**

84 *Bat Capture and Sampling*

85 We captured 740 Madagascar fruit bats (314 *Eidolon dupreanum*, 201 *Pteropus rufus,*
86 225 *Rousettus madagascariensis*) across four sites in 18 discrete sampling events between
87 November 2013 and January 2016 using methods that have been previously described (Brook
88 et al., 2015). Captured animals were measured, weighed, sexed, thumb-tagged, and
89 categorized by broad age/reproductive class. Between 0.03 and 1ml of blood (no more than
90 1% of the animal's body mass) was collected from the brachial vein of each captured bat,
91 centrifuged and stored separately as serum and pelleted blood cell. A subset of adult bats (85
92 *P. rufus* and 90 *E. dupreanum*) were processed under anesthesia using a halothane vaporizer
93 (4% halothane in oxygen at 0.7L/min), and a lower left premolar tooth was extracted from
94 these individuals for aging purposes. *R. madagascariensis* bats were deemed too small for
95 tooth extraction and therefore not subject to anesthesia or aging.

Additionally, researchers at the Institut Pasteur of Madagascar (IPM) captured, sexed, weighed, measured, and serum-sampled 440 *E. dupreanum* bats between November 2005 and July 2007 (Iehlé et al., 2007). We included measurement and serostatus data from these capture events in our Aim 1 and 2 analyses.

Ethics Statement

All field work was carried out in accordance with guidelines posted by the American Veterinary Medical Association and under permit authorization from the Madagascar Ministry for Water and Forests (sampling permit #: 166/14/MEF/SG/ DGF/DCB.SAP/SCB, 75/15/MEEMEF/SG/DGF/DCB.SAP/SCB, 92/16/MEEMEF/SG/ DGF/DCB.SAP/SCB, 259/16/MEEF/SG/DGF/DSAP/SCB). All field protocols employed were pre-approved by the Princeton University Institutional Animal Care and Use Committee (IACUC Protocol # 1926), and every effort was made to minimize discomfort to animals.

Sample Processing and Serological Analysis

Aging

Tooth samples were exported and processed histologically at Matson's Laboratory (Missoula, Montana), following previously published protocols (Cool, Bennet, & Romaniuk, 1994; Divljan, Parry-Jones, & Wardle, 2006), to yield integer estimates of age via *cementum annuli* counts. Because fruit bats birth in annual pulses (Peel et al., 2014), we obtained more precise estimates of age by assuming a standard birth date for captured bats of a given species and adding the duration of time between capture and birth date to the integer estimate of age via *cementum annuli*. We computed ages for pups less than one year in the same way. In Madagascar, births are staggered amongst the three species, with the largest, *P. rufus,*

120 birthing first, followed by *E. duprenaum* and *R. madagascariensis* (Andrianaivoarivelo,
121 2015), though the latter were not aged in our study. Assuming respective birth dates of
122 October 1 and November 1, we computed age to the nearest day for 142 *P. rufus* and 109 *E.*
123 *dupreanum.*
124
125 *Luminex-based Serological Assay*
126 Serum samples were screened for antibodies against henipavirus and filovirus soluble
127 glycoproteins (Hendra: HeV sG, HeV sF; Nipah: NiV sG, NiV sF; Cedar: CedPV sG, CedV
128 sF; Ebola: EBOV sGp, and Marburg: MARV sGp) using a Luminex-based, Bio-Plex®
129 (BioRad, Inc.) assay that has been previously described (Bossart et al., 2007; Chowdhury et
130 al., 2014; Hayman et al., 2008; Peel et al., 2012, 2013) (Text S1).
131 For the 2005-2007 Institut Pasteur subset of data, samples were screened for
132 antibodies to NiV and HeV henipaviruses by standard enzyme-linked immunosorbent assay
133 (ELISA). Only serostatus (no raw titers) were made available, and we accepted the original
134 researchers' classification of individuals as seropositive or seronegative.
135
136 **Quantitative Analysis**
137 *Aim 1: Henipa- and filovirus spp. exposure*
138 This investigation represents the first application of our Luminex assay to serum
139 samples collected from Madagascar bats, meaning that no definitive positive or negative
140 controls for any species examined were available. Instead, following previously published
141 methods (Burroughs et al., 2016; Peel et al., 2013; Trang et al., 2015), we fit finite mixture
142 models to the natural log of the MFI data to approximate a cutoff MFI value (and

143 corresponding upper and lower confidence interval) for seropositivity for each
144 species/antigen combination (Text S2; Table S1, S2; Fig. S1).
145 Because our antigens were not originally obtained from Madagascar fruit bats, we
146 required that each species/antigen data subset meet several additional criteria before further
147 statistical analysis. For each data subset, we required that MFI values either (a) show
148 correlation with an $R^2 > 40\%$ for associated soluble glycoproteins within the same viral
149 genus (an indicator of reliable cross-reactivity among antibodies to related viruses; Fig. S2),
150 (b) have values > 1000 MFI for some individual[s] assayed (Gombos et al., 2013) and/or (c)
151 result in > 10% seroprevalence based on the mixture model cutoff (Text S3). We summarize
152 all serological data, in conjunction with age and sampling data in Table S3 of the Supporting
153 Information.
154
155 *Aim 2: Seasonality in seroprevalence and serostatus*
156 We next aimed to identify any seasonal trends in population-level seroprevalence or
157 individual serostatus for antigens which met the criteria outlined under Aim 1. We restricted
158 these analyses to adult-sized bats over one year in age from our own data, combined with *E.*
159 *dupreanum* data from IPM (Iehlé et al., 2007). We analyzed each species/antigen subset of
160 our data separately for a total of seven independent analyses (see Results, Table 1). For each
161 data subset, we fit a separate Generalized Additive Model (GAM) in the binomial family,
162 using a matrix of seropositive/seronegative counts by sampling event as the response variable
163 and mid-date of sampling event as the smoothing predictor, with a random effect of site and
164 year. All GAMs were fit via REML estimation, and we fixed the number of smoothing knots
165 (k) at seven, as recommended by the package author (Wood, 2001). *R. madagascariensis*
166 data were too sparse to permit model convergence at k=7; in these cases, we fixed k at 6.

167 Once each model was fit, we used the predict.gam() function to obtain a predicted
168 estimate of seroprevalence by sampling event, bounded by an upper and lower 95%
169 confidence interval. We list the basic structural forms of all GAMs considered in Text S4 and
170 summarize outputs from fitted binomial GAMs in Table S4 (Fig. S3).

171 We next reformatted our data to examine seasonality within a calendar year,
172 independent of year of study. We used binomial GAMs to test for seasonality in serostatus
173 for adult bats of both sexes and all three species. We set a matrix of seropositive by
174 seronegative counts per Julian day-of-year as our response variable, as computed from mean,
175 lower, and upper MFI thresholds for seropositivity, and modeled antigen type as the fixed
176 predictor and day-of-year as the smoothing predictor. We used a "by" term to enable a
177 separate smoother for each sex. All models included random effects of capture site and year.
178 Because we investigated broad seasonal fluctuations, we restricted the number of smoothing
179 knots (*k*) to four and used a cyclic cubic regression spline which forces the smoother to
180 transition continuously from the end of one year to the beginning of the next (Text S4; Table
181 S5; Fig. S4).

182 Additionally, 17 unique *E. dupreanum* individuals (three female, 14 male) were
183 captured twice across the duration of our study. Of the two *E. dupreanum* antigens that met
184 criteria for statistical analysis (see Results, Table 1), only anti-NiV-G titers demonstrated
185 substantial dynamism among recaptures. Data were too few for meaningful statistical
186 analysis, but we nonetheless interpreted results anecdotally (Fig. S5).

187 Finally, we used Gaussian GAMs to test for seasonality in mass: forearm residual for
188 adult bats within a given year. The mass: forearm residual gives a crude measure of body
189 condition by which to compare bat 'health' within a given sex and species. Bats above the
190 mass: forearm length regression line are "heavier" and those below the line "lighter" than

predicted, suggestive of over- and under-nourished conditions—though we caution that we did not validate this inference by comparing measured "mass" with quantification of body lipid content (Pearce, O'Shea, & Wunder, 2008).

We first established a standardized mass: forearm residual for all adult bats in our dataset by (a) dividing the raw mass per individual by the mean mass of that particular species and sex, then (b) regressing standardized mass against forearm length, and (c) calculating the residual from the species-specific linear model (Fig. S6). We used "standard major axis" type 2 linear regression in this analysis since we anticipated variation and error in measurements for both x and y-axes (Legendre, 2014). We then modeled these data with standardized mass: forearm residual as the response variable and Julian day-of-year as the smoothing predictor, including random effects of site and year and a cyclic cubic regression spline (Text S4; Table S6).

Aim 3: Comparing mechanistic hypotheses

Finally, to recover the mechanistic underpinnings of our data, we fit a series of epidemiological models, encompassing a suite of bat virus transmission hypotheses, to longitudinal NiV-G age-seroprevalence data for *E. dupreanum* and to EBOV-Gp seroprevalence for *P. rufus*. For this final research aim, analyses were restricted to the 109 *E. dupreanum* and 142 *P. rufus* samples for which we possessed age estimates; for the purposes of model-fitting, we further sub-sampled age-seroprevalence data to include only those individuals captured at our longitudinally-resampled Moramanga site. We evaluated each age-seroprevalence sub-sample for representativeness of the broader sampling event from which it was derived using bootstrapping techniques (Text S3) and ultimately fit models to serological data from 72 aged *E. dupreanum* and 123 aged *P. rufus* (Table S3).

215 All models were constructed using discrete-time, age-structured, matrix modeling
216 techniques for epidemics (Klepac & Caswell, 2011; Klepac et al., 2009; C.J.E. Metcalf et al.,
217 2012), assuming frequency-dependent transmission, homogeneous mixing, and equilibrium
218 structure across age classes (Text S5). We considered variations on five discrete model
219 structures: (a) MSIR, (b) MSRIR, (c) MSIRS, (d) MSIRN, and (e) MSIRNR. In all cases, we
220 modeled the 'M' (maternally immune; Fig. S7) and 'R' (recovered) classes as seropositive.
221 The (a) MSIR (maternally-immune, susceptible, infectious, recovered) model represents a
222 classic paradigm in the dynamics of transmission for many perfectly-immunizing infections,
223 offering a null hypothesis against which to compare other dynamical structures (Bjornstad,
224 Finkenstadt, & Grenfell, 2002; Metcalf et al., 2012; Metcalf, Bjørnstad, Grenfell, &
225 Andreasen, 2009). The simplest extension, (b) MSRIR, allows bats to seroconvert directly
226 into the R-class without becoming demonstrably infectious, as has been shown in the
227 experimental literature (Jones et al., 2015; J. T. Paweska et al., 2015). The (c) MSIRS model
228 permits waning immunity and return of recovered individuals to susceptible status, offering
229 one possible explanation for the intermittent pulses of bat viral excretion posited to underpin
230 spillover events (Amman et al., 2012; Plowright et al., 2015, 2011, 2016). The (d) MSIRN
231 model allows for antibody waning of seropositive bats from the R-class into a seronegative
232 but still immune class, 'N', which could represent either non-antibody-mediated immunity or
233 sub-seropositive antibody titers that still remain protective, again reflecting the experimental
234 literature (Paweska et al., 2016; Schuh et al., 2017). The (e) MSIRNR model merely extends
235 MSIRN to allow N-class bats to return to seropositivity after re-challenge and renewed
236 contact with infectious individuals.
237 Other work has suggested that pulses in bat viral transmission may result from SILI-
238 like (susceptible, infectious, latent, infectious) within-host dynamics. Optimization of a SILI

model would require finescale recapture data documenting live virus infection across individual bats sampled longitudinally; lacking this, we instead approximated longitudinal serological variation in MSIRN/MSIRNR model forms, which allow for dynamic antibody titers post initial seroconversion.

In all modeled epidemics, populations were jointly subjected to survival and epidemic transitions. Births were subsequently introduced into the population but restricted in duration to a 10-week, species-specific annual period. Births were distributed among the four or five epidemic states, according to parental effects: we assumed that S-class bats of reproductive age (≥ two years) produced Susceptible offspring, while I- and R-class bats of reproductive age produced Maternally immune offspring. We tested model forms both by which N-class dams produced S- ("matSus") and M-class ("matAB") offspring.

We controlled demographic rates under assumptions of stable age structure (annual adult survival = .793 for *E. dupreanum* and .511 for *P. rufus*; annual juvenile survival = .544; annual birth rate = .48 for both species). In keeping with previously developed multi-state matrix models for human diseases (Metcalf et al., 2011, 2012; Wesolowski et al., 2016), we modeled epidemic processes on a biweekly (14-day) timescale, such that twenty-six survival-epidemic transitions were permitted across a given year. In all cases, we assumed homogenous mixing across age classes and a constant transmission coefficient (β) across the duration of the time series (though the force of infection, λ, nonetheless cycled annually in conjunction with changes in the infectious population). We fixed the recovery rate from infection at one biweek^{-1}, the average of rates approximated in the literature (Hayman, 2015; Paweska et al., 2012; Swanepoel et al., 1996) and optimized all other epidemic parameters, depending on the chosen model structure, by minimizing the negative log-likelihood of data of a specific age and biweek, given the model's output at that same age and time. For all

263 models, we fit rates for waning of maternally-inherited antibodies (ω) and transmission (β)
264 held constant across age and time (Table S7). For MSIRS, MSIRN, and MSIRNR models,
265 we additionally fit a waning antibody rate for individuals exiting the R class (σ); for MSRIR
266 models, a rate of direct seroconversion from S to R (ρ); and for MSIRNR models, a rate of
267 antibody boosting (γ), by which bats returned to R from N. For MSIRN/R models, we
268 explored variations in model structure under which N-class dams produced either Maternally
269 immune (-matAB) or Susceptible young (-matSus). All seven models were re-fit six different
270 times: to NiV-G/*E. dupreanum* and EBOV-Gp/*P. rufus* data at all three MFI thresholds for
271 seropositivity, to yield 42 distinct sets of parameter estimations.
272
273 **Results**
274 *Aim 1: Henipa- and filovirus spp. exposure*
275 In all, seven species/antigen combinations met criteria for further analysis, indicating
276 the presence of reliable reactive antibodies to tested antigens in serum from species in
277 question: NiV-G and CedPV-G in *E. dupreanum*, HeV-F and EBOV-Gp in *P. rufus*, and
278 HeV-F, CedPV-G, and EBOV-Gp in *R. madagascariensis* (Table 1, S2). These Luminex
279 results indicate that all three Madagascar fruit bat species demonstrated antibody reactivity to
280 Hendra and/or Nipah-related henipaviruses; the inclusion of *R. madagascariensis* represents
281 an expansion on previous findings (Iehlé et al., 2007; Table 1). MFI values from the NiV-
282 G/HeV-G and NiV-F/HeV-F Luminex assays were highly correlated (Fig. S2), suggesting
283 cross-reactivity against related Nipah/Hendra-like henipavirus antigens. For each species, we
284 selected the Nipah/Hendra-like antigen that yielded the highest MFI per species for further
285 ecological analysis: NiV-G for *E. dupreanum* and HeV-F for *P. rufus* and *R.*
286 *madagascariensis* (Table 1).

Table 1. Seroprevalence to henipa- and filovirus antigens in Madagascar fruit bats†

Species	Virus	N	Viral Antigen Assayed	Max MFI	MFI Cutoff mean [lci*, uci**]	Seroprevalence % (N pos)		
						At mean cutoff	At lci* cutoff	At uci** cutoff
Eidolon dupreanum	Cedar	314	CedPV-G	2436.3	166.46 [95.68, 374.55]	0.64 (2)	1.27 (4)	0.64 (2)
	Hendra/ Nipah††	**314**	**NiV-G**	**6553**	**402.90 [225.50, 1506.48]**	**24.2 (76)**	**32.17 (101)**	**10.19 (32)**
Pteropus rufus	Hendra/ Nipah	201	HeV-G	439.3	67.55 [61.29, 77.58]	5.47 (11)	6.97 (14)	3.48 (7)
	Ebola††	**201**	**EBOV-Gp**	**697.5**	**110.49 [90.58, 284.02]**	**10.4 (21)**	**12.94 (26)**	**4.48 (9)**
Rousettus madagascariensis	Cedar	225	CedV-F	623.8	75.75 [70.17, 84.00]	8.44 (19)	9.33 (21)	7.11 (16)
	Hendra/ Nipah	225	HeV-F	437.3	77.46 [68.75, 94.77]	7.56 (17)	8.44 (19)	6.67 (15)
	Ebola	225	EBOV-Gp	5716	457.76 [358.52, 552.07]	8.44 (19)	12 (27)	6.67 (15)

†Seroprevalence here indicates evidence of pathogen exposure found in current (2013-2016) field studies; historical data from 2005-2007 is not included here. Results from species-virus combinations for which no seropositives were recovered (*E. dupreanum*: Marburg/Ebola, *P. rufus:* Cedar/Marburg, *R. madagascariensis:* Marburg) are shown in Table S2.

††Of these antigen/species combinations shown here, **two (in bold)** met more restrictive criteria for age-seroprevalence analyses. We report only results for NiV-G in *E. dupreanum* in the main text of the manuscript.

*lci = lower confidence interval threshold for the MFI cutoff for seropositivity. This is a more lenient threshold than the mean.

**uci = upper confidence interval threshold for the MFI cutoff for seropositivity. This is a stricter threshold than the mean.

Additionally, we document the first serological evidence of cross-reactivity with a third henipavirus, Cedar virus, in *E. dupreanum* and *R. madagascariensis*, although seroprevalences were low (anti-CedPV-G and anti-CedV-F seroprevalence = 1.27% and 9.33%, respectively). We also report the first serological evidence of filovirus exposure in any Madagascar wildlife. Samples from both *P. rufus* and *R. madagascariensis* tested seropositive to Ebola (EBOV-Gp) but not Marburg (MARV-Gp) virus antigen, while all *E. dupreanum* samples assayed seronegative to EBOV-Gp and MARV-Gp. We compiled individual serostatus by all three MFI cutoffs to compute seroprevalences for all species/antigen combinations across 33 discrete sampling events in our study (Table S3).

297 Because ages were unavailable for *R. madagascariensis*, and seroprevalences were
298 low for HeV-F in *P. rufus* and CedPV-G in *E. dupreanum* (6.97% and 1.27% respectively),
299 we restricted mechanistic modeling of age-seroprevalence trends (Aim 3) to NiV-G in *E.*
300 *dupreanum* and EBOV-Gp in *P. rufus* data only. Due to concerns over the lack of specificity
301 and validation in our assay for EBOV-Gp in *P. rufus* (which met only one of our three
302 criteria for analysis), we ultimately reported results for these fits in the Supporting
303 Information only and reserved the main text of our manuscript for modeling of anti-NiV-G in
304 *E. dupreanum* data, which met all three of criteria for analysis. This Luminex has been
305 previously validated on samples from the sister species *E. helvum* (Hayman et al., 2008; Peel
306 et al., 2018).
307
308 *Aim 2: Seasonality in seroprevalence and serostatus*
309 Generalized additive modeling indicated significant seasonal trends for henipavirus
310 seroprevalence (NiV-G) in the *E. dupreanum* time series and for ebolavirus spp.
311 seroprevalence (EBOV-Gp) in the *P. rufus* time series (Fig. 1; Fig. S3; Table S4).
312 Population-level seroprevalences appeared to increase across the gestation period for *E.*
313 *dupreanum* anti-NiV-G and *R. madagascariensis* anti-EBOV-Gp data. Seasonal patterns
314 were clearest in the 2005-2007 Institut Pasteur de Madagascar (IPM) subset of the *E.*
315 *dupreanum* anti-NiV-G data, demonstrating biannual peaks in seroprevalence at the height of
316 the wet season and the end of gestation.

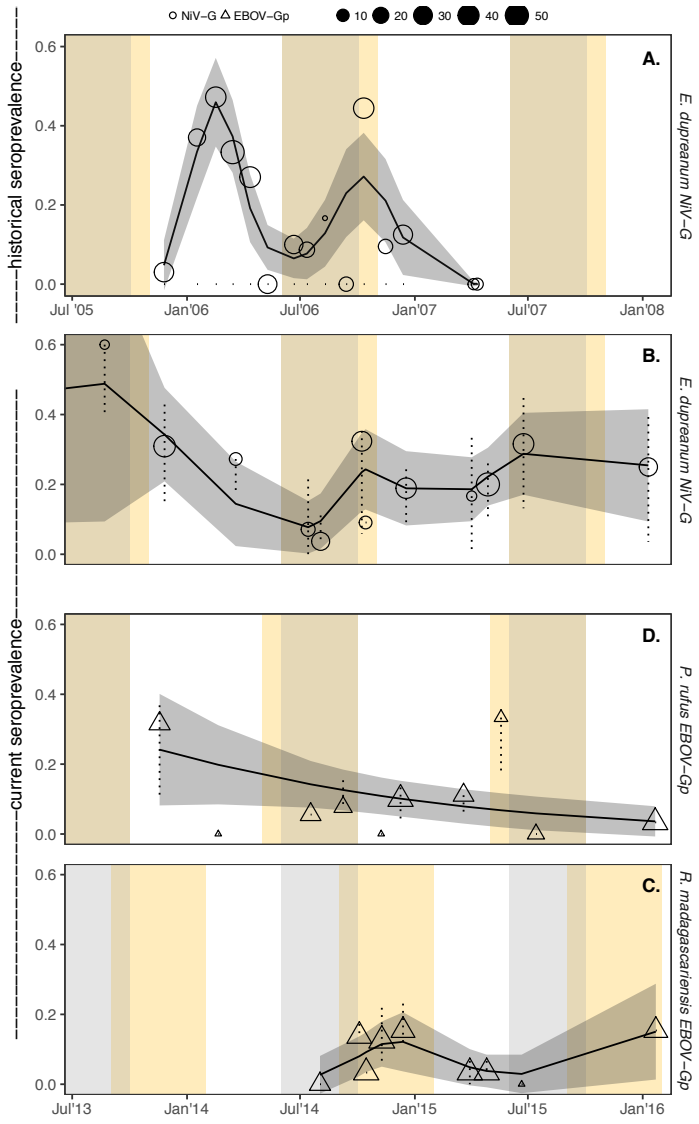

Fig. 1. ***Seasonality in seroprevalence***
(A) Predicted NiV-G seroprevalence by sampling date for *E. dupreanum,* across range of historically-sampled 2005-2007 data. The nutrient-poor Madagascar dry season is highlighted in gray vertical shading and the species-specific gestation period in yellow. Solid line and shaded 95% confidence intervals give the predicted seroprevalence from a significant binomal GAM construction of seropositive vs. seronegative by sampling date with random effects silenced for visualization purposes only. Data (with 95% exact binomial confidence intervals) are shown as open shapes in the background; shape size is correlated with sample size (as indicated in the legend). Analyses are repeated across the date range of the authors' current studies in **(B)**, **(C)**, **(D)** for NiV-G in *E. dupreanum,* EBOV-Gp in *P. rufus,* and EBOV-Gp in *R. madagascariensis,* respectively. GAM constructions and results are summarized in Text S4 and Table S4. Seasonal smoothers by date (incorporating random effects) are significant for *E. dupreanum* and *P. rufus* data (panels **A-C**). Seasonal trends in seroprevalence for other species/antigen combinations in Table 1 are summarized in Fig. S3.

333 Additional GAMs constructed using Julian day-of-year as a predictor indicated
334 significant seasonality in seropositive status for female *E. dupreanum* and *R.*
335 *madagascariensis* (Fig. 2 A-C; Table S5). Female *P. rufus* did not exhibit significant
336 seasonality in serostatus, although the periodicity of the smoothing trend recovered from this
337 model correlated with those from other species. Serostatus for certain antigens (NiV-G in
338 *E.dupreanum,* EBOV-Gp in *P.* rufus and HeV-F in *R. madagascariensis*) tracked
339 reproduction, increasing across gestation for females (time-lagged among the three species),
340 then decreasing post-birth and through lactation and weaning.

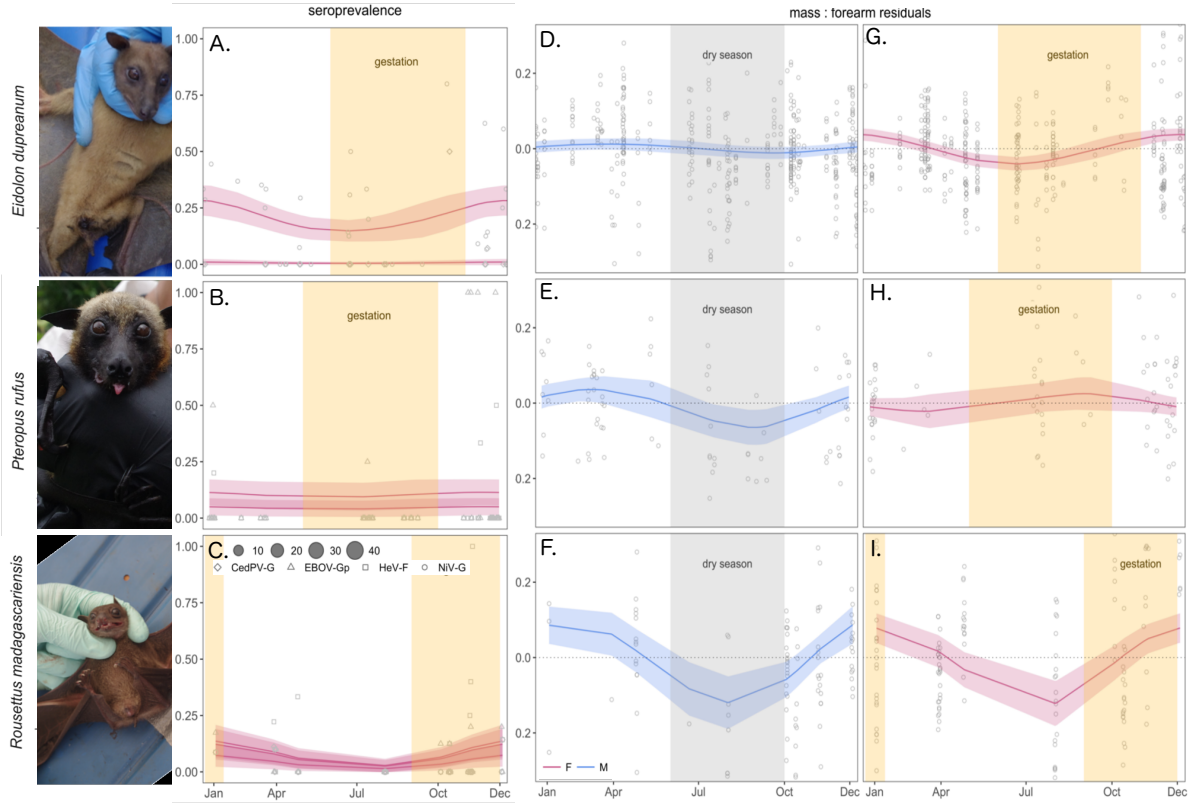

341

342 **Fig. 2.** ***Seasonality in seroprevalence and body mass:forearm residual***
343 Seasonal seroprevalence by discrete antigen in **(A)** female *E. dupreanum,* **(B)** *P. rufus,* and
344 **(C)** *R. madagascariensis* bats. Seasonal mass:forearm residual in, respectively, male and
345 female **(D, G)** *E. dupreanum,* **(E, H)** *P. rufus,* and **(F, I)** *R. madagascariensis* bats. The
346 species-specific gestation period is highlighted in yellow shading on the female plots and the
347 nutrient-poor Madagascar dry season in gray shading on the male plots. Solid lines (pink =
348 female; blue = male) show the predicted seroprevalence for each antigen (A-C) and the
349 predicted mass : forearm residual (D-I) from GAMs. Note that lines for seroprevalence for
350 different antigens within a species (A-C) are indistinguishable; however, the top line for *E.*

dupreanum (A) corresponds to anti-NiV-G seroprevalence, for *P. rufus* (B) to anti-EBOV-Gp seroprevalence, and for *R. madagascariensis* (C) to anti-HeV-F seroprevalence. Data for raw seroprevalence per sampling event (with 95% exact binomial confidence intervals) are shown as open shapes in the background (shape type corresponds to antigen, as indicated in legend). Raw mass:forearm residual data are shown, by month, in the background for each sampled individual (open circles) in D-I. Note that *E. dupreanum* data are combined with 2005-2007 sampling data from Institut Pasteur de Madagascar. Full GAM constructions are reported in Text S4 and results summarized in Table S5. The insignificant seasonal smoother for male serostatus and corresponding seroprevalence data are shown in Fig. S4.

Male bats did not exhibit significant seasonality in seroprevalence at the population level (Fig. S4), though three of fourteen recaptured male and one of three recaptured female *E. dupreanum* demonstrated dynamic anti-NiV-G titers (Fig. S5). Using the mean MFI cutoff, one adult male bat (unknown age), originally captured at the end of the dry season and recaptured at the close of the subsequent wet season, had transitioned from seronegative to seropositive (titers increased by >800 MFI). A second adult male (unknown age), caught first in the middle of the wet season, showed titers elevated by >700 MFI when recaught at the onset of the dry season but tested seropositive in both samplings. A third adult male (aged ~8.75 yrs), caught first in the middle of the dry season, showed *decreased* titers by ~200 MFI upon recapture a few months later into the dry season. Finally, a lactating female bat (unknown age) showed decreased titers by ~700 MFI after weaning her pup prior to recapture.

Seasonal smoothers incorporated into GAMs predicting annual variation in mass: forearm residual were significant for females of all three species and for *P. rufus* and *R. madagascariensis* males (but not for *E. duprenaum* males; Table S6). As with serostatus, seasonal periodicity in mass: forearm residual tracked reproduction for females—increasing across gestation, then declining post-birth and through lactation. For males, the seasonal smoother synchronously tracked the nutritional calendar: mass: forearm residual increased across Madagascar's fruit-abundant wet season, then declined through the nutrient-poor dry

380 season. Female mass: forearm residuals were not corrected for pregnancy. The majority of
381 female adult fruit bats give birth to one pup each year; Hayman et al. (2012) report that 96%
382 of adult age female *Eidolon helvum* give birth annually in Ghana. The gain in female mass:
383 forearm residual across gestation exhibited in our data thus likely reflects a gain in fetal mass
384 rather than improved body condition for the mother.

385 All told, these patterns suggest a significant seasonal component to serostatus for
386 female Madagascar fruit bats, correlated with the reproductive calendar. Females are more
387 likely to be seropositive during gestation (overlapping the dry Malagasy winter). No
388 significant seasonal changes in male serostatus were observed in GAM-analyzed population-
389 level data; however, data from recaptured individuals suggest that antibody titers in male bats
390 declined subtly across the dry season and increased again throughout the wet season when
391 male bats were at peak body mass.

392

393 *Aim 3: Comparing mechanistic hypotheses*

394 Teeth were processed histologically to yield integer estimates of fruit bat age (see
395 Methods), producing species-specific age-frequency distributions for *E. dupreanum* and *P.*
396 *rufus* (Fig. 3). Adult mortality rates derived from exponential models fit to *E. dupreanum*
397 data are compatible with assumptions of stable population structure, but age-frequencies
398 recovered for *P. rufus* indicate that the species is likely in serious population decline. As
399 such, we adopted juvenile mortality rates from *E. dupreanum* for epidemiological modeling
400 of *P. rufus* data (Text S5). We combined age data with serological data amassed under Aim 1
401 to develop age-seroprevalence curves for NiV-G in *E. dupreanum* and EBOV-Gp in *P. rufus*
402 (Text S5).

403

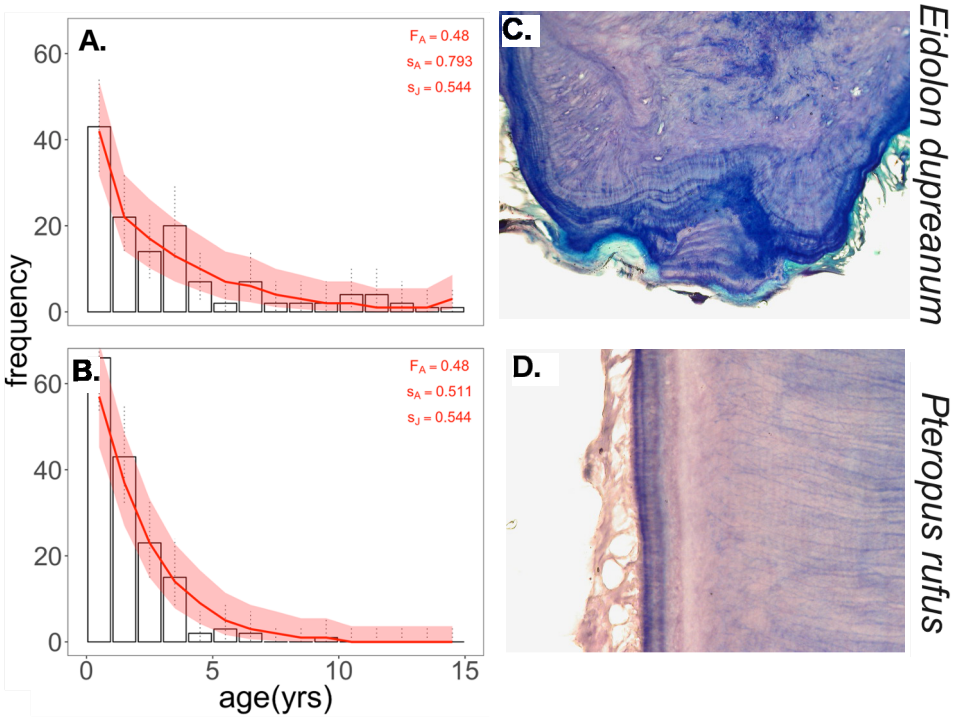

Fig. 3. ***Aging Madagascar fruit bats via*** **cementum annuli. (A)** Age-frequency distribution generated from *cementum annuli* counts of extracted *E. dupreanum* teeth. Histogram is binned by year, with 95% exact binomial confidence intervals shown as dotted lines. The red curve is the predicted age frequency distribution generated from the fit of a simple exponential model to age distribution > 6 months, incorporating an annual adult survival rate of .793 and a juvenile annual survival rate of .544 (determined using Leslie matrix techniques to maintain a stable age distribution and constant population size; Text S5). Translucent shading shows 95% confidence intervals of the exponential fit by standard error. **(B)** Age-frequency distribution from *cementum annuli* counts of extracted *P. rufus* teeth, with a fitted exponential model (red line) and 95% confidence intervals (red shading), incorporating an annual adult survival rate of .511 and a juvenile survival rate of .544 (constant population size was impossible for *P. rufus,* so we adopted the same rate as for *E. dupreanum;* Text S5). **(C)** Stained *cementum annuli* from a 14-year-old *E. dupreanum* sample. **(D)** Stained *cementum annuli* from a 2-year-old *P. rufus.*

Composite age-seroprevalence data for *E. dupreanum* NiV-G demonstrated high seroprevalence in neonates, suggestive of inherited maternal antibodies (Text S5; Fig. S7). This neonatal seroprevalence peak decreased rapidly following presumed waning of maternal immunity, then increased across early life, before tapering off once more in later age classes (Fig. 4). When examined longitudinally, data demonstrated a decay in neonatal seroprevalence across the year, as pups' maternally-inherited immunity waned following the birth pulse (Fig. S8, S9). The neonatal decline and early age increase in seroprevalence in our

427 data replicates patterns previously reported for NiV-G exposure in African *E. helvum* (Peel et
428 al., 2018), but our observed late-age seroprevalence decline contrasts with the late-age
429 plateau of anti-NiV-G seroprevalence in the African system. We recovered similar age-
430 seroprevalence patterns of EBOV-Gp exposure in *P. rufus* (Text S5; Fig. S10-12).

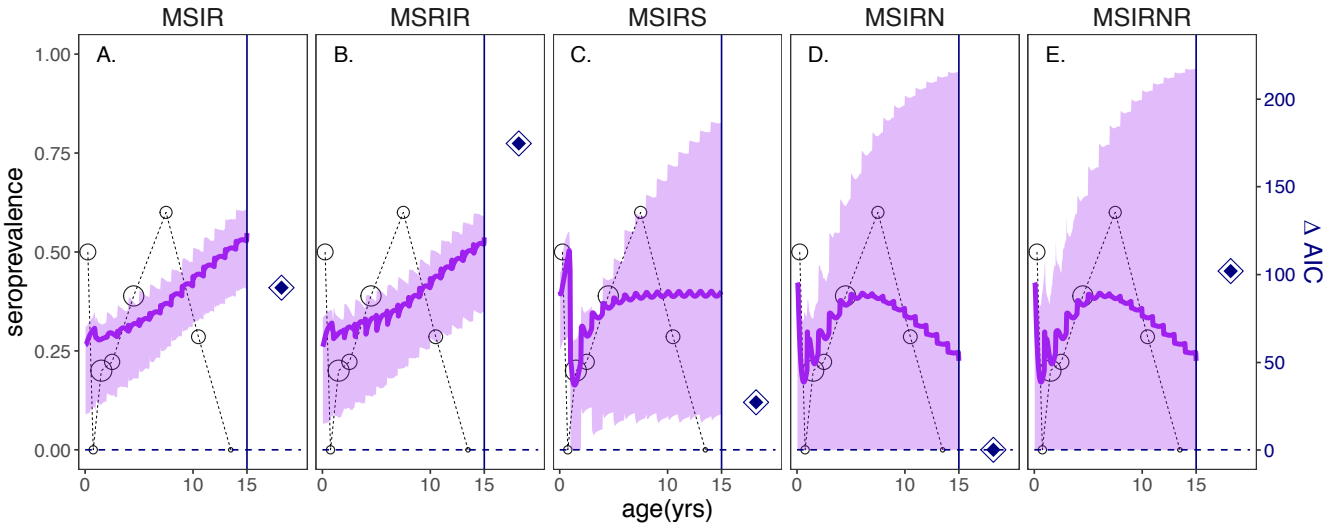

431
432 **Fig. 4.** ***Model fits to age-seroprevalence data***
433 Age-seroprevalence curves for *E. dupreanum* NiV-G, using the mean MFI cutoff for
434 seropositive status. Seroprevalence data (left y-axis) are shown as open circles, binned for 0-
435 .5 yrs, .5-1 yrs, 1-1.5yrs, 1.5-3 yrs, and for 3-yr increments increasing after that. Shape size
436 corresponds to the number of bats sampled per bin (respective sample sizes, by age bin, are:
437 N=10,2,20,9,18,5,7,1). Solid purple lines indicate model outputs, and translucent shading
438 highlights the 95% confidence interval derived from the Hessian matrix of the maximum
439 likelihood of each model fit to the data. Panels are stratified into columns by model structure:
440 **(A)** MSIR = Maternally immune, Susceptible, Infectious, Recovered; **(B)** MSRIR=
441 Maternally immune, Susceptible, Recovered via direct seroconversion, Infectious,
442 Recovered; **(C)** MSIRS = Maternally immune, Susceptible, Infectious, Recovered,
443 Susceptible; **(D)** MSIRN= Maternally immune, Susceptible, Infectious, Recovered, Non-
444 antibody immune; **(E)** MSIRNR = Maternally immune, Susceptible, Infectious, Recovered,
445 Non-antibody immune; Recovered). All MSIRN/R model outputs depicted assume that Non-
446 antibody immune dams produce Maternally immune-class young. The right-hand y-axis (in
447 navy) of each subplot shows ΔAIC for each model fit, relative to all other models in the
448 figure (navy diamonds). The MSIRN model (D) offered the best fit to the data, corresponding
449 to ΔAIC = 0. All parameter values, confidence intervals, and raw AIC scores for each model
450 fit are reported in Table S7. Model fits including MSIRN/R fits assuming N-class mothers
451 produce susceptible young are shown in Fig. S10, along with fits to seroprevalence data for
452 *P. rufus*-EBOV-Gp. Fits calculated using the lower and upper MFI thresholds for
453 seropositivity are shown in Figs S11-12.
454

We report composite age-seroprevalence data for *E. dupreanum* NiV-G, combined with model outputs summarized across one age-structured equilibrium year, in Fig. 4 (Fig. S10). The right-hand panel in each subplot shows relative AIC within a given data subset; raw AIC scores are listed in Table S7. Compared to all other model structures, the MSIRN model most effectively recaptured data for both species under all putative MFI cutoffs when assuming that N-class mothers produced M-class young ("matAB"). Results for model specifications in which N-class mothers produced S-class pups are additionally reported in Fig. S10-12 and Table S7. Only MSIRN/R models effectively reproduced late-age declines in seroprevalence (with MSIRNR performing too poorly in AIC comparison for true consideration as a best fit model), while MSIRS predicted a late-age seroprevalence plateau.

Parameter estimates varied between the two best fit models: MSIRN-matAB and MSIRS. No empirical measurements of bat virus transmission (against which to compare β estimates) are available in the literature, but MSIRN models fit to the mean MFI cutoff for *E. dupreanum* NiV-G recovered optimized values for the rate of waning maternal immunity, ω (0.12 biweek^{-1}, corresponding to a maternal antibody duration of four months), and the rate of waning adult humoral immunity, σ (.01 biweek^{-1}, corresponding to an adult antibody duration of four years), within the range previously reported in the literature for African *E. helvum* (six months for maternal immunity and four years for adult humoral immunity) (Epstein et al., 2013; Peel et al., 2018). MSIRS models produced considerably higher optimized parameter values, indicating shorter durations of maternal antibodies (two weeks) and adult humoral immunity (two years). Such rapid rates of antibody waning were essential to avoid increasing seroprevalence with age but, arguably, less biologically defensible. AIC values, parameter estimates, and confidence intervals for models fit to all three MFI cutoffs, as well as to the *P. rufus* EBOV-Gp data, are summarized in Table S7.

479 **Discussion**

480 We leveraged henipa- and filovirus serological data for three species of wild
481 Malagasy fruit bat to evaluate support for contrasting mechanisms hypothesized to drive
482 longitudinal, seasonal viral and immune dynamics in this system. Though Plowright et al.
483 (2016) cautioned that, "inference from serology alone is unlikely to differentiate
484 among…proposed epidemiological scenarios" for mechanisms underpinning population-level
485 patterns in bat virus data, the serological analysis methods employed here nonetheless narrow
486 the range of plausible competing hypotheses considerably and simultaneously underscore
487 critical knowledge gaps that could be addressed in future field studies. Our analysis of age-
488 structured serological data highlights several key insights: (1) we expand globally on the
489 known range of bat hosts for henipaviruses and filoviruses, (2) we demonstrate seasonal
490 patterns in population-level seroprevalence and individual-level serostatus for Malagasy fruit
491 bats, concomitant with the reproductive calendar, and (3) we use mechanistic models to
492 reveal the critical role of waning humoral immunity and the potential for alternative immune
493 processes in governing serological patterns witnessed in our data.

494 We report many serological findings novel for the Madagascar ecosystem—including
495 the first evidence of antibodies cross-reactive with Cedar henipavirus (CedPV-G: *E.*
496 *dupreanum* and CedV-F: *R. madagascariensis*) and Zaire ebolavirus antigens (*P. rufus* and
497 *R. madagascariensis*) in any wild Malagasy host. The documentation of bat antibodies cross-
498 reactive with Zaire ebolavirus (but not Marburg) antigen will interest the global public health
499 community, as recent work classes Madagascar within the "zoonotic niche" of both Ebola
500 (Pigott et al., 2014; Schmidt et al., 2017) and Marburg (Pigott et al., 2015) filoviruses.
501 Ironically, Madagascar's inclusion in these risk maps has been largely derived from the
502 species distribution of *Eidolon dupreanum* (Han et al., 2016; Pigott et al., 2014), the one

503 Malagasy fruit bat for which we found no filovirus seropositive samples. This finding is not
504 hugely surprising if we consider the relative rarity of Ebola seropositivity in *E. dupreanum*'s
505 sister taxon, *E. helvum* (Olival & Hayman, 2014), which possesses a receptor-level
506 substitution that makes it refractory to Ebola infection (Ng et al., 2015).

507 Given Madagascar's geographic isolation and the considerable phylogenetic distance
508 separating its fruit bats from their nearest mainland relatives (Almeida et al., 2014; Goodman
509 et al., 2010; Shi et al., 2014), it seems likely that some of the seropositives recovered in this
510 study result from cross-reactivity of Malagasy bat antibodies to related-but-distinct antigens
511 from those assayed here. To date, no henipaviruses or filoviruses have been identified (via
512 live virus or RNA) in Madagascar. Detection and characterization of these viruses, together
513 with description of the specificity, avidity, and neutralization capacity of their antibodies,
514 thus represents a critical research priority. The probable cross-reactivity of Malagasy bat
515 antibodies derived from different—and potentially novel—henipa- and filovirus antigens
516 adds considerable uncertainty to our tabulation of MFI thresholds for seropositivity.

517 The greatest challenge to our dynamical inference is the possibility that seropositive
518 samples do not signify true circulating virus within any of our three species. In laboratory
519 trials, for example, *R. aegyptiacus* bats are known to seroconvert upon contact with
520 inoculated individuals without ever becoming detectably infectious (Jones et al., 2015;
521 Paweska et al., 2015). While we attempted to explore these dynamics within a single bat
522 population using our MSRIR model, it is possible that focal viruses circulate in species
523 distinct from those studied here, resulting in seropositive samples via dead-end
524 seroconversion from transient bat contact with an alternative reservoir. Although we cannot
525 falsify this hypothesis, there are a few specifics of the Madagascar ecosystem that make such
526 a scenario unlikely. In particular, all but one of the roosts surveyed in this study are largely

527 single-species conglomerations: *P. rufus* is a tree-dwelling pteropodid which only roosts in
528 single-species assemblages, while *E. dupreanum* predominantly inhabits cracks and
529 crevasses with conspecifics (Goodman, 2011). In cave environments, *E. dupreanum* and *R.*
530 *madagascariensis* occasionally co-roost and roost with insectivorous bats (Cardiff,
531 Ratrimomanarivo, Rembert, & Goodman, 2009), and all three fruit bat species contact at
532 feeding sites. Nonetheless, given the relative rarity of these cross-species contacts, it is
533 unlikely that the high seroprevalence recovered in our data for anti-NiV-G antibodies in *E.*
534 *dupreanum* (24.2%) and anti-EBOV-Gp antibodies in *P. rufus* (10.2%) result from dead-end
535 seroconversion alone. Previous work has investigated paramyxovirus spp. by PCR among
536 insectivorous bats in Madagascar (Wilkinson et al., 2014, 2012), and no henipavirus spp.
537 have been identified, further supporting our assumptions that Malagasy fruit bats maintain
538 their own endemic viral transmission cycles.

539 The lack of specificity in our serological assay also permits the possibility that a
540 given bat population might maintain active infections with multiple serologically
541 indistinguishable viruses of the same family, which are nonetheless epidemiologically
542 unique; serum from Ebola-infected humans, for example, will recognize all five known
543 species of ebolavirus (MacNeil, Reed, & Rollin, 2011). An analysis like ours would consider
544 serological evidence of any ebolavirus infection equivalently and model all seropositives as
545 one population, though, in reality, each specimen could represent a distinct virus that
546 maintains its own transmission cycle. Again, we cannot falsify this hypothesis, but recent
547 molecular work supports a theory of single-bat, single-filovirus species interactions that runs
548 counter to this claim (Ng et al., 2015). We observed vast differences in the range of MFI
549 titers recovered for each antigen amongst our three bat species, recovering high MFI titers for
550 EBOV-Gp in *R. madagascariensis* but only mid-range titers in *P. rufus* (Table 1). We also

551 found that *E. dupreanum* serum reacted most strongly to the NiV-G antigen, while *P. rufus*
552 and *R. madagascariensis* serum bound more tightly to the HeV-F antigen. Such differences
553 could be attributable to cross-species variation in the robustness of the humoral immune
554 response or could indicate that our tested antigens more closely align with the wild antigen
555 from which one species' antibodies were derived vs. that of another. This species-specific
556 variation in antibody binding to the same antigen challenge supports our decision to model
557 each bat species-virus relationship independently, rather than allowing for significant inter-
558 species transmission to govern viral dynamics in this system.

559 Female serostatus for both henipavirus and filovirus spp. varied seasonally in our
560 data, tracking reproduction for *E. dupreanum* and *R. madagascariensis*; female bats showed
561 elevated antibody titers during reproduction, consistent with previous work (Baker et al.,
562 2014). This pattern suggests that viral control is one of many costs to which resource-limited
563 hosts must allocate energy and that male and female bats do so differently while facing
564 distinct metabolic demands. While higher serotiters in reproductive females may seem
565 counterintuitive if viewed as increased investment in immunity, recent research suggests that
566 bats may control viral infections primarily via innate immune pathways (Zhou et al., 2016),
567 which are more metabolically costly than adaptive immunity (Raberg et al., 2002). It is
568 possible then that female bats trade off innate immunity with less metabolically demanding
569 means of viral control (i.e. antibodies) during reproductive periods (Brook & Dobson, 2015),
570 or that contact rates with infectious individuals are elevated during these seasons, resulting in
571 antibody-boosting effects (*e.g.* Paweska et al., 2015; Schuh et al., 2017). Alternatively,
572 elevated antibody titers might be independent of both exposure and metabolic tradeoffs; for
573 example, production of the milk protein prolactin (typically elevated in late pregnancy and

early lactation for mammals) is known to stimulate antibody production and facilitate maternal antibody transfer to young (Spangelo, Hall, Ross, & Goldstein, 1987).

Males, with fewer reproductive constraints, demonstrate no clear shifts in seasonal serostatus at the population-level. Nonetheless, recapture data suggest that male antibody titers subtly track seasonal peaks and troughs in body mass, increasing during the fruit-abundant wet season and declining during the dry season. Understanding seasonal tradeoffs in bat immune investment will be critical to enhancing our capacity for predicting seasonal pulses in viral transmission and informing possible zoonotic risk. Paired field studies, tracking viral excretion in conjunction with individual serostatus, will be essential to elucidating these dynamics in the future.

One of the largest questions arising from our investigation addresses the extent to which seropositive status correlates with infectiousness and immunity. Previous work highlights notable seasonality in spillover of both Hendra (Plowright et al., 2015) and Ebola viruses (Schmidt et al., 2017), although the mechanistic contributions of bat demography versus physiology remain unclear. In our models, the force of infection varied seasonally as a result of birth pulse-mediated cycles in the infectious population (Fig. S13). Seasonal fluctuations in the magnitude of transmission—which could emerge from changes in host contact rates (Ferrari et al., 2008; Grenfell, Bjornstad, & Finkenstadt, 2002), variation in within-host immunological susceptibility (Dowell, 2001), or periodicity in viral shedding (Plowright et al., 2015)—might further modulate seasonality in FOI. Several studies have highlighted the possible role that latent infections and viral recrudescence could play in bat virus transmission (Plowright et al., 2016; Rahman et al., 2011), but data from longitudinally resampled individuals were too few to allow for evaluation of any such model in our study. If future field work is able to demonstrate a role for seasonal transmission independent of

demography, then the extent to which observed seasonality in serotiter could serve as a biomarker for an individual bat's infectiousness or susceptibility will be critical to resolving predictive power from cross-sectional serological data.

We fit age-structured, epidemic models to age-seroprevalence data and recovered strong support for models incorporating waning humoral immunity (i.e. MSIRS, MSIRN). This result is consistent with previous experimental findings, which demonstrate rapidly declining antibody titers in Marburg-infected *R. aegyptiacus,* post inoculation and seroconversion (Paweska et al., 2015; Schuh et al., 2017). In our system, we can eliminate the hypothesis by which simple SIR dynamics incorporating a seasonal birth pulse might drive seasonality in viral shedding (Plowright et al., 2016); such a model yields a pattern of monotonically increasing seroprevalence with age at odds with our data. In our analysis, the MSIRN model consistently outperformed all other tested models in fits to the data, when constructed such that N-class dams produce M-class offspring. We hypothesize that N-class serotiters could be dynamic: N-class females may exhibit seasonally elevated seropositive titers during reproduction (consistent with findings from Aim 2), then subsequently reduce titers to seronegative levels post-gestation.

In a few cases in our analysis, the late age seroprevalence plateau predicted by the MSIRS model was statistically indistinguishable from the decline predicted by MSIRN, likely due to low sample sizes among older age individuals. More extensive sampling will be needed to parse whether the seroprevalence decline witnessed in our dataset holds. Recent modeling of age-seroprevalence trends for NiV-G in *E. helvum* suggests that, in the African system at least, seroprevalence plateaus at older ages, consistent with MSIRS dynamics (Peel et al., 2018), though it is possible that late-age susceptibles in this system were captured during low titer periods in seasonally dynamic N-class individuals. With our present data, we

622 are unable to adequately distinguish between MSIRS and MSIRN hypotheses—and unable to
623 assess the plausibility of an MSILI hypothesis—but both the experimental literature and our
624 findings under Aim 2 suggest that the dynamics of humoral immunity post-initial
625 seroconversion are likely more complex than a complete return to the susceptible class would
626 assume. Field and laboratory studies tracking viral pathogenesis in individual bats are greatly
627 needed to enable construction of accurate within-host models and to reduce our reliance on
628 difficult-to-obtain wildlife age data (Borremans, Hens, Beutels, Leirs, & Reijniers, 2016;
629 Pepin et al., 2017). More nuanced within-host models might, for example, incorporate
630 multiple classes for seropositive bats, differentiated by MFI value: R-class individuals could
631 have extremely high MFIs, while N-class individuals might have titers at some intermediate
632 level. At present, there is a tradeoff in selecting an MFI cutoff conservative enough to limit
633 potential for false positives and lenient enough not to miss true seropositives with dynamic
634 titers. If, in the future, chiropteran immunologists successfully develop assays capable of
635 distinguishing N-class bats (for example, some marker of cell-mediated immunity),
636 construction of age-N-prevalence curves would be illuminating. We would expect MSIRN
637 dynamics to yield patterns of monotonically increasing N-prevalence with age, while MSIRS
638 and MSIRNR assumptions would yield age-N-prevalence plateaus.

639 Finally, we note that late age declines in seroprevalence can be recaptured under
640 assumptions of infection-induced mortality (*e.g.* Williams, Gouws, Wilkinson, & Karim,
641 2001). Preliminary experimentation with such model forms indicated that they were unable
642 to more effectively recapture our data than those simpler model constructions investigated
643 here, making this added complexity statistically unjustifiable. To date, no study has yet
644 demonstrated any clinical signature of infection-induced morbidity or mortality in bats
645 naturally or experimentally infected with henipa- or filoviruses (Amman et al., 2012; Jones et

al., 2015; Paweska et al., 2012; Schuh et al., 2017; Williamson et al., 1998; Williamson, Hooper, Selleck, Westbury, & Slocombe, 2000). Although we chose not to explore models of this form at this time, we caution that we should remain cognizant of these possibility mechanisms in the future.

Although no known bat-borne zoonoses have been documented in Madagascar, our work confirms a history of exposure to potentially zoonotic henipaviruses and filoviruses in several widespread, endemic fruit bat species. These species are widely consumed throughout Madagascar, and the majority of bat hunting—and corresponding bat-human contact—is concentrated during the resource-poor winter, overlapping with bat gestation and elevated anti-viral seroprevalence in our data (Golden et al., 2014; Jenkins et al., 2011; Jenkins & Racey, 2008). If seasonal changes in serostatus are revealed to have any bearing on viral transmission, insights from our modeling will offer a predictive framework to safeguard public health.

Acknowledgements

We gratefully acknowledge Tony Fooks, Animal & Plant Health Agency, U.K., the Institut Pasteur de Madagascar, and the Madagascar Institute for the Conservation of Tropical Ecosystems (MICET) for logistical support on this project. We thank Yan-Ru Feng and Lianying Yan for producing and supplying the viral glycoprotein Bioplex beads and control monoclonal antibodies and Lalaina Nomenjanahary, Yun-Yun-Li, and Miora Rasolomanantsoa for help in the field. We thank Bryan Grenfell, Andrea Graham, the Graham lab at Princeton University for valuable commentaries on this work. The opinions or assertions contained herein are the private ones of the authors and are not to be construed as official or reflecting the views of the Department of Defense, the Department of the Navy, or the Uniformed Services University of the Health Sciences, and no official endorsement should be inferred.

Author Contributions

CEB, JMH, CJM, and APD conceived the ideas and designed methodology. CEB and HCR collected the field data. CCB, AAC, and JLNW designed the Luminex serological platform. LG carried out the serological assays. CEB analyzed all data with input from AJP, CJM, and APD. CCB, AAC, JMH, and JLNW contributed materials and reagents. CEB led the writing of the manuscript. All authors contributed critically to the drafts and gave final approval for publication.

Data accessibility:

All data for analyses described in this manuscript are including in tables of the Supporting Information attached to this manuscript.

694 **References**

695 Almeida, F. C., Giannini, N. P., Simmons, N. B., & Helgen, K. M. (2014). Each flying fox
696 on its own branch: a phylogenetic tree for *Pteropus* and related genera (Chiroptera:
697 Pteropodidae). *Molecular Phylogenetics and Evolution*, (March).
698 doi:10.1016/j.ympev.2014.03.009
699 Amman, B. R., Carroll, S. A., Reed, Z. D., Sealy, T. K., Balinandi, S., Swanepoel, R., …
700 Towner, J. S. (2012). Seasonal pulses of Marburg virus circulation in juvenile *Rousettus*
701 *aegyptiacus* bats coincide with periods of increased risk of human infection. *PLoS*
702 *Pathogens*, *8*(10), e1002877. doi:10.1371/journal.ppat.1002877
703 Amman, B. R., Jones, M. E. B., Sealy, T. K., Uebelhoer, L. S., Schuh, A. J., Bird, B. H., …
704 Towner, J. S. (2014). Oral shedding of Marburg virus in experimentally infected
705 Egyptian Fruit Bats (*Rousettus aegyptiacus*). *Journal of Wildlife Diseases*, *51*(1).
706 doi:10.7589/2014-08-198
707 Andrianaivoarivelo, R. (2015). Personal communication.
708 Baker, K. S., Suu-Ire, R., Barr, J., Hayman, D. T. S., Broder, C. C., Horton, D. L., … Wood,
709 J. L. N. (2014). Viral antibody dynamics in a chiropteran host. *Journal of Animal*
710 *Ecology*, *83*(2), 415–428. doi:10.1111/1365-2656.12153
711 Bjornstad, O. N., Finkenstadt, B. F., & Grenfell, B. T. (2002). Dynamics of measles
712 epidemics: Estimating scaling of transmission rates using a times series SIR model.
713 *Ecological Monographs*, *72*(2), 169–184.
714 Blackwood, J. C., Streicker, D. G., Altizer, S., & Rohani, P. (2013). Resolving the roles of
715 immunity, pathogenesis, and immigration for rabies persistence in vampire bats.
716 *Proceedings of the National Academy of Sciences of the United States of America*,
717 *110*(51), 20837–42. doi:10.1073/pnas.1308817110

718 Borremans, B., Hens, N., Beutels, P., Leirs, H., & Reijniers, J. (2016). Estimating time of
719 infection using prior serological and individual information can greatly improve
720 incidence estimation of human and wildlife infections. *PLoS Computational Biology*,
721 *12*(5), e1004882. doi:10.1371/journal.pcbi.1004882
722 Bossart, K. N., McEachern, J. A., Hickey, A. C., Choudhry, V., Dimitrov, D. S., Eaton, B. T.,
723 & Wang, L. F. (2007). Neutralization assays for differential henipavirus serology using
724 Bio-Plex Protein Array Systems. *Journal of Virological Methods*, *142*(1–2), 29–40.
725 doi:10.1016/j.jviromet.2007.01.003
726 Brook, C. E., Bai, Y., Dobson, A. P., Osikowicz, L. M., Ranaivoson, H. C., Zhu, Q., &
727 Kosoy, M. Y. (2015). *Bartonella* spp. in fruit bats and blood-feeding ectoparasites in
728 Madagascar. *PLoS Neglected Tropical Diseases*, *10*(2), e0003532.
729 doi:10.1371/journal.pntd.0003532
730 Brook, C. E., Bai, Y., Yu, E. O., Ranaivoson, H. C., Shin, H., Dobson, A. P., … Dittmar, K.
731 (2017). Elucidating transmission dynamics and host-parasite-vector relationships for
732 rodent-borne *Bartonella* spp. in Madagascar. *Epidemics*, *20*, 56–66.
733 doi:10.1016/j.epidem.2017.03.004
734 Brook, C. E., & Dobson, A. P. (2015). Bats as 'special' reservoirs for emerging zoonotic
735 pathogens. *Trends in Microbiology*, *23*(3), 172–80. doi:10.1016/j.tim.2014.12.004
736 Brook, C. E., Ranaivoson, H. C., Andriafidison, D., Ralisata, M., Razafimanahaka, J.,
737 Heraud, J.-M., … Metcalf, C. J. (2019). Age-based inference into population trends for
738 Madagascar fruit bats. *Bioogical Conservation*.
739 Burroughs, A. L., Durr, P. A., Boyd, V., Graham, K., White, J. R., Todd, S., … Wang, L. F.
740 (2016). Hendra virus infection dynamics in the grey-headed flying fox (*Pteropus*
741 *poliocephalus*) at the southern-most extent of its range: Further evidence this species

742 does not readily transmit the virus to horses. *PLoS ONE*, *11*(6), 1–18.
743 doi:10.1371/journal.pone.0155252
744 Calisher, C. H., Childs, J. E., Field, H. E., Holmes, K. V, & Schountz, T. (2006). Bats:
745 Important reservoir hosts of emerging viruses. *Clinical Microbiology Reviews*, *19*(3),
746 531–45. doi:10.1128/CMR.00017-06
747 Cardiff, S. G., Ratrimomanarivo, F. H., Rembert, G., & Goodman, S. M. (2009). Hunting,
748 disturbance and roost persistence of bats in caves at Ankarana, northern Madagascar.
749 *African Journal of Ecology*, *47*(4), 640–649. doi:10.1111/j.1365-2028.2008.01015.x
750 Chowdhury, S., Khan, S. U., Crameri, G., Epstein, J. H., Broder, C. C., Islam, A., … Luby,
751 S. P. (2014). Serological evidence of henipavirus exposure in cattle, goats and pigs in
752 Bangladesh. *PLoS Neglected Tropical Diseases*, *8*(11), e3302.
753 doi:10.1371/journal.pntd.0003302
754 Cool, S. M., Bennet, M. B., & Romaniuk, K. (1994). Age estimation of pteropodid bats
755 (Megachiroptera) from hard tissue parameters. *Wildlife Research*, *21*(3), 353.
756 doi:10.1071/WR9940353
757 Divljan, A., Parry-Jones, K., & Wardle, G. M. (2006). Age determination in the grey-headed
758 flying fox. *Journal of Wildlife Management*, *70*(2), 607–611.
759 Dowell, S. F. (2001). Seasonal variations in host suceptibility and cycles of certain infectious
760 diseases. *Emerging Infectious Diseases*, *7*(3), 369–374. doi:10.3201/eid0703.017301
761 Epstein, J. H., Baker, M. L., Zambrana-Torrelio, C., Middleton, D., Barr, J. A., DuBovi, E.,
762 … Daszak, P. (2013). Duration of maternal antibodies against Canine Distemper Virus
763 and Hendra virus in Pteropid bats. *PLoS ONE*, *8*(6), 1–8.
764 doi:10.1371/journal.pone.0067584
765 Epstein, J. H., Prakash, V., Smith, C. S., Daszak, P., McLaughlin, A. B., Meehan, G., …

766 Cunningham, A. a. (2008). Henipavirus infection in fruit bats (*Pteropus giganteus*),
767 India. *Emerging Infectious Diseases*, *14*(8), 1309–11. doi:10.3201/eid1408.071492
768 Farrington, C. P. (1990). Modelling forces of infection for measles, mumps, and rubella.
769 *Statistics in Medicine*, *9*(August 1989), 953–967.
770 Ferrari, M. J., Grais, R. F., Bharti, N., Conlan, A. J. K., Bjørnstad, O. N., Wolfson, L. J., …
771 Grenfell, B. T. (2008). The dynamics of measles in sub-Saharan Africa. *Nature*,
772 *451*(7179), 679–84. doi:10.1038/nature06509
773 Golden, C. D., Bonds, M. H., Brashares, J. S., Rodolph Rasolofoniaina, B. J., & Kremen, C.
774 (2014). Economic valuation of subsistence harvest of wildlife in Madagascar.
775 *Conservation Biology*, 1–10. doi:10.1111/cobi.12174
776 Gombos, P., Opelz, G., Scherer, S., Morath, C., Zeier, M., Schemmer, P., & Süsal, C. (2013).
777 Influence of test technique on sensitization status of patients on the kidney transplant
778 waiting list. *American Journal of Transplantation*, *13*(8), 2075–2082.
779 doi:10.1111/ajt.12332
780 Goodman, S. M. (2011). *Les chauves-souris de Madagascar [in French]*. Antananarivo,
781 Madagascar: Association Vahatra.
782 Goodman, S. M., Chan, L., Nowak, M., & Yoder, A. D. (2010). Phylogeny and biogeography
783 of western Indian Ocean *Rousettus* (Chiroptera : Pteropodidae). *Journal of Mammalogy*,
784 *91*(3), 593–606. doi:10.1644/09-MAMM-A-283.1.Key
785 Grenfell, B. T., & Anderson, R. M. (1985). The estimation of age-related rates of infection
786 from case notifications and serological data. *The Journal of Hygiene*, *95*(2), 419–36.
787 Retrieved from
788 http://www.pubmedcentral.nih.gov/articlerender.fcgi?artid=2129533&tool=pmcentrez&
789 rendertype=abstract

790 Grenfell, B. T., Bjornstad, O. N., & Finkenstadt, B. F. (2002). Dynamics of measles
791 epidemics: Scaling noise, determinism, and predictability with the TSIR Model.
792 *Ecological Monographs*, *72*(2), 185–202.
793 Griffiths, D. A. (1974). A catalytic model of infection for measles. *Journal of the Royal*
794 *Statistical Society, Series C*, *23*(3), 330–339.
795 Halpin, K., Hyatt, A. D., Fogarty, R., Middleton, D., Bingham, J., Epstein, J. H., … Daszak,
796 P. (2011). Pteropid bats are confirmed as the reservoir hosts of henipaviruses: a
797 comprehensive experimental study of virus transmission. *The American Journal of*
798 *Tropical Medicine and Hygiene*, *85*(5), 946–51. doi:10.4269/ajtmh.2011.10-0567
799 Han, B. A., Schmidt, J. P., Alexander, L., Bowden, S. E., Hayman, D. T. S., & Drake, J. M.
800 (2016). Undiscovered bat hosts of filoviruses. *PLoS Neglected Tropical Diseases*, *in*
801 *review*, 1–10. doi:10.6084/m9.figshare.3114310
802 Hayman, D. T. S. (2015). Biannual birth pulses allow filoviruses to persist in bat populations.
803 *Proceedings of the Royal Society B*, *282*(20142591). doi:10.1098/rspb.2014.2591
804 Hayman, D. T. S., Emmerich, P., Yu, M., Wang, L.-F., Suu-Ire, R., Fooks, A. R., … Wood,
805 J. L. N. (2010). Long-term survival of an urban fruit bat seropositive for Ebola and
806 Lagos bat viruses. *PloS One*, *5*(8), e11978. doi:10.1371/journal.pone.0011978
807 Hayman, D. T. S., McCrea, R., Restif, O., Suu-Ire, R., Fooks, A. R., Wood, J. L. N., …
808 Rowcliffe, J. M. (2012). Demography of straw-colored fruit bats in Ghana. *Journal of*
809 *Mammalogy*, *93*(5), 1393–1404. doi:10.1644/11-MAMM-A-270.1
810 Hayman, D. T. S., Suu-Ire, R., Breed, A. C., McEachern, J. A., Wang, L., Wood, J. L. N., &
811 Cunningham, A. A. (2008). Evidence of henipavirus infection in West African fruit
812 bats. *PloS One*, *3*(7), e2739. doi:10.1371/journal.pone.0002739
813 Heisey, D. M., Joly, D. O., & Messier, F. (2006). The fitting of general force-of-infection

models to wildlife disease prevalence data. *Ecology*, *87*(9), 2356–2365.

Hens, N., Aerts, M., Faes, C., Shkedy, Z., Lejeune, O., Damme, P. Van, & Beutels, P. (2010). 75 years of estimating the force of infection. *Epidemiology and Infection*, *1*(c), 1–32. doi:10.1017/CBO9781107415324.004

Iehlé, C., Razafitrimo, G., Razainirina, J., Andriaholinirina, N., Goodman, S. M., & Faure, C. (2007). Henipavirus and Tioman virus antibodies in Pteropodid bats, Madagascar. *Emerging Infectious Diseases*, *13*(1), 159–161.

Jenkins, R. K. B., Keane, A., Rakotoarivelo, A. R., Rakotomboavonjy, V., Randrianandrianina, F. H., Razafimanahaka, H. J., … Jones, J. P. G. (2011). Analysis of patterns of bushmeat consumption reveals extensive exploitation of protected species in eastern Madagascar. *PloS One*, *6*(12), e27570. doi:10.1371/journal.pone.0027570

Jenkins, R. K. B., & Racey, P. A. (2008). Bats as bushmeat in Madagascar. *Madagascar Conservation and Development*, *3*(1), 22–30.

Jones, M., Schuh, A., Amman, B., Sealy, T., Zaki, S., Nichol, S., & Towner, J. (2015). Experimental inoculation of Egyptian rousette bats (*Rousettus aegyptiacus*) with viruses of the Ebolavirus and Marburgvirus genera. *Viruses*, *7*(7), 3420–3442. doi:10.3390/v7072779

Klepac, P., & Caswell, H. (2011). The stage-structured epidemic: Linking disease and demography with a multi-state matrix approach model. *Theoretical Ecology*, *4*(3), 301–319. doi:10.1007/s12080-010-0079-8

Klepac, P., Pomeroy, L. W., Bjørnstad, O. N., Kuiken, T., Osterhaus, A. D. M. E., & Rijks, J. M. (2009). Stage-structured transmission of phocine distemper virus in the Dutch 2002 outbreak. *Proceedings. Biological Sciences / The Royal Society*, *276*(1666), 2469–2476. doi:10.1098/rspb.2009.0175

838 Legendre, P. (2014). lmodel2: Model II Regression. R package version 1.7-2.

839 Leroy, E. M., Kumulungui, B., Pourrut, X., Rouquet, P., Hassanin, A., Yaba, P., …
840 Swanepoel, R. (2005). Fruit bats as reservoirs of Ebola virus. *Nature*, *438*(7068), 575–6.
841 doi:10.1038/438575a

842 Long, G. H., Sinha, D., Read, A. F., Pritt, S., Kline, B., Harvill, E. T., … Bjørnstad, O. N.
843 (2010). Identifying the age cohort responsible for transmission in a natural outbreak of
844 Bordetella bronchiseptica. *PLoS Pathogens*, *6*(12). doi:10.1371/journal.ppat.1001224

845 MacNeil, A., Reed, Z., & Rollin, P. E. (2011). Serologic cross-reactivity of human IgM and
846 IgG antibodies to five species of Ebola virus. *PLoS Neglected Tropical Diseases*, *5*(6).
847 doi:10.1371/journal.pntd.0001175

848 Mathiot, C. C., Fontenille, D., Georges, A. J., & Coulanges, P. (1989). Antibodies
849 populations to haemorrhagic fever viruses in Madagascar. *Transactions of the Royal*
850 *Society of Tropical Medicine and Hygiene*, *83*, 407–409.

851 Metcalf, C. J. E., Bjørnstad, O. N., Ferrari, M. J., Klepac, P., Bharti, N., Lopez-Gatell, H., &
852 Grenfell, B. T. (2011). The epidemiology of rubella in Mexico: seasonality, stochasticity
853 and regional variation. *Epidemiology and Infection*, *139*(7), 1029–1038.
854 doi:10.1017/S0950268810002165.The

855 Metcalf, C. J. E., Bjørnstad, O. N., Grenfell, B. T., & Andreasen, V. (2009). Seasonality and
856 comparative dynamics of six childhood infections in pre-vaccination Copenhagen.
857 *Proceedings of the Royal Society B*, *276*(1676), 4111–8. doi:10.1098/rspb.2009.1058

858 Metcalf, C. J. E., Lessler, J., Klepac, P., Morice, A., Grenfell, B. T., & Bjørnstad, O. N.
859 (2012). Structured models of infectious disease: Inference with discrete data.
860 *Theoretical Population Biology*, *82*(4), 275–282. doi:10.1016/j.tpb.2011.12.001

861 Middleton, D. J., Morrissy, C. J., van der Heide, B. M., Russell, G. M., Braun, M. A.,

862 Westbury, H. A., … Daniels, P. W. (2007). Experimental Nipah virus infection in
863 pteropid bats (*Pteropus poliocephalus*). *Journal of Comparative Pathology*, *136*(4),
864 266–72. doi:10.1016/j.jcpa.2007.03.002
865 Muench, H. (1959). *Catalytic models in epidemiology.* Boston, MA, USA: Harvard
866 University Press.
867 Munster, V. J., Adney, D. R., van Doremalen, N., Brown, V. R., Miazgowicz, K. L., Milne-
868 Price, S., … Bowen, R. A. (2016). Replication and shedding of MERS-CoV in Jamaican
869 fruit bats (*Artibeus jamaicensis*). *Scientific Reports*, *6*(August 2015), 21878.
870 doi:10.1038/srep21878
871 Ng, M., Ndungo, E., Kaczmarek, M., Herbert, A. S., Binger, T., James, R., … Chandran, K.
872 (2015). NPC1 contributes to species-specific patterns of Ebola virus infection in bats.
873 *ELife*, 1–22. doi:10.7554/eLife.11785
874 Ogawa, H., Miyamoto, H., Nakayama, E., Yoshida, R., Nakamura, I., Sawa, H., … Takada,
875 A. (2015). Seroepidemiological prevalence of multiple species of filoviruses in fruit bats
876 (*Eidolon helvum*) migrating in Africa. *Journal of Infectious Diseases*, 1–8.
877 doi:10.1093/infdis/jiv063
878 Olival, K., & Hayman, D. (2014). Filoviruses in bats: Current knowledge and future
879 directions. *Viruses*, *6*(4), 1759–1788. doi:10.3390/v6041759
880 Olival, K. J., Hosseini, P. R., Zambrana-Torrelio, C., Ross, N., Bogich, T. L., & Daszak, P.
881 (2017). Host and viral traits predict zoonotic spillover from mammals. *Nature*.
882 doi:10.1038/nature22975
883 Paweska, J., Storm, N., Grobbelaar, A., Markotter, W., Kemp, A., & Jansen van Vuren, P.
884 (2016). Experimental inoculation of Egyptian fruit bats (*Rousettus aegyptiacus*) with
885 Ebola Virus. *Viruses*, *8*(2), 29. doi:10.3390/v8020029

886 Paweska, J. T., Jansen van Vuren, P., Fenton, K. A., Graves, K., Grobbelaar, A. A., Moolla,
887 N., … Kemp, A. (2015). Lack of Marburg virus transmission from experimentally
888 infected to susceptible in-contact Egyptian fruit bats. *Journal of Infectious Diseases*, 1–
889 10. doi:10.1093/infdis/jiv132
890 Paweska, J. T., Jansen van Vuren, P., Masumu, J., Leman, P. A., Grobbelaar, A. A.,
891 Birkhead, M., … Kemp, A. (2012). Virological and serological findings in *Rousettus*
892 *aegyptiacus* experimentally inoculated with Vero cells-adapted Hogan strain of Marburg
893 virus. *PloS One*, *7*(9), e45479. doi:10.1371/journal.pone.0045479
894 Pearce, R. D., O'Shea, T. J., & Wunder, B. A. (2008). Evaluation of morphological indices
895 and total body electrical conductivity to assess body composition in big brown bats.
896 *Acta Chiropterologica*, *10*(1), 153–159. doi:10.3161/150811008X331171
897 Peel, A. J., Baker, K. S., Crameri, G., Barr, J. A., Hayman, D. T., Wright, E., … Wood, J. L.
898 N. (2012). Henipavirus neutralising antibodies in an isolated island population of
899 African fruit bats. *PloS One*, *7*(1), e30346. doi:10.1371/journal.pone.0030346
900 Peel, A. J., Baker, K. S., Hayman, D. T. S., Broder, C. C., Cunningham, A. A., Fooks, A. R.,
901 … Restif, O. (2018). Support for viral persistence in bats from age-specific serology and
902 models of maternal immunity. *Scientific Reports*, *8*(1), 3859. doi:10.1038/s41598-018-
903 22236-6
904 Peel, A. J., McKinley, T. J., Baker, K. S., Barr, J. A., Crameri, G., Hayman, D. T. S., …
905 Wood, J. L. N. (2013). Use of cross-reactive serological assays for detecting novel
906 pathogens in wildlife: Assessing an appropriate cutoff for henipavirus assays in African
907 bats. *Journal of Virological Methods*, *193*(2), 295–303.
908 doi:10.1016/j.jviromet.2013.06.030
909 Peel, A. J., Pulliam, J. R. C., Luis, A. D., Plowright, R. K., Shea, T., Hayman, D. T. S., …

910 Restif, O. (2014). The effect of seasonal birth pulses on pathogen persistence in wild
911 mammal populations. *Proceedings of the Royal Society B*, *281*, 20132962.
912 Pepin, K. M., Kay, S., Golas, B., Shriner, S., Gilbert, A., Miller, R., … Buhnerkempe, M.
913 (2017). Inferring infection hazard in wildlife populations by linking data across
914 individual and population scales. *Ecology Letters*. doi:10.1111/ele.12732
915 Pigott, D. M., Golding, N., Mylne, A., Huang, Z., Henry, A. J., Weiss, D. J., … Hay, S. I.
916 (2014). Mapping the zoonotic niche of Ebola virus disease in Africa. *ELife*, *3*(December
917 2013), 1–29. doi:10.7554/eLife.04395
918 Pigott, D. M., Golding, N., Mylne, A., Huang, Z., Weiss, D. J., Brady, O. J., … Hay, S. I.
919 (2015). Mapping the zoonotic niche of Marburg virus disease in Africa. *Transactions of*
920 *the Royal Society of Tropical Medicine and Hygiene*, 1–13. doi:10.1093/trstmh/trv024
921 Plowright, R. K., Eby, P., Hudson, P. J., Smith, I. L., Westcott, D., Bryden, W. L., …
922 McCallum, H. (2015). Ecological dynamics of emerging bat virus spillover.
923 *Proceedings of the Royal Society B*, *282*(1798). doi:10.1098/rspb.2014.2124
924 Plowright, R. K., Field, H. E., Smith, C., Divljan, A., Palmer, C., Tabor, G., … Foley, J. E.
925 (2008). Reproduction and nutritional stress are risk factors for Hendra virus infection in
926 little red flying foxes (*Pteropus scapulatus*). *Proceedings of the Royal Society B:*
927 *Biological Sciences*, *275*(1636), 861–9. doi:10.1098/rspb.2007.1260
928 Plowright, R. K., Foley, P., Field, H. E., Dobson, A. P., Foley, J. E., Eby, P., & Daszak, P.
929 (2011). Urban habituation, ecological connectivity and epidemic dampening: the
930 emergence of Hendra virus from flying foxes (Pteropus spp.). *Proceedings. Biological*
931 *Sciences / The Royal Society*, *278*(1725), 3703–12. doi:10.1098/rspb.2011.0522
932 Plowright, R. K., Peel, A. J., Streicker, D. G., Gilbert, A., McCallum, H., Wood, J., … Restif,
933 O. (2016). Transmission or within-host dynamics driving pulses of zoonotic viruses in

934 reservoir-host populations. *PLoS Neglected Tropical Diseases*, 1–21.
935 doi:10.1371/journal.pntd.0004796
936 Pomeroy, L. W., Bjornstad, O. N., Kim, H., Jumbo, S. D., Abdoulkadiri, S., & Garabed, R.
937 (2015). Serotype-specific transmission and waning immunity of endemic foot-and-
938 mouth disease virus in Cameroon. *PLoS ONE*, *10*(9), 1–16.
939 doi:10.1371/journal.pone.0136642
940 Raberg, L., Vestberg, M., Hasselquist, D., Holmdahl, R., Svensson, E., & Nilsson, J. A.
941 (2002). Basal metabolic rate and the evolution of the adaptive immune system.
942 *Proceedings of the Royal Society B: Biological Sciences*, *269*(1493), 817–821.
943 doi:10.1098/rspb.2001.1953
944 Rahman, A. S., Hassan, L., Sharifah, S. H., Lazarus, K., Zaini, C. M., Epstein, J. H., …
945 Daszak, P. (2011). Evidence for Nipah virus recrudescence and serological patterns of
946 captive *Pteropus vampyrus*. *Epidemiology and Infection*, *139*(10), 1570–9.
947 doi:10.1017/S0950268811000550
948 Schmidt, J. P., Park, A. W., Kramer, A. M., Han, B. A., Alexander, L. W., & Drake, J. M.
949 (2017). Spatiotemporal fluctuations and triggers of Ebola virus spillover. *Emerging*
950 *Infectious Diseases*, *23*(3), 415–422. doi:10.3201/eid2303.160101
951 Schuh, A. J., Amman, B. R., Jones, M. E. B., Sealy, T. K., Uebelhoer, L. S., Spengler, J. R.,
952 … Towner, J. S. (2017). Modelling filovirus maintenance in nature by experimental
953 transmission of Marburg virus between Egyptian rousette bats. *Nature Communications*,
954 *8*, 14446. doi:10.1038/ncomms14446
955 Schuh, A. J., Amman, B. R., Sealy, T. K., Spengler, J. R., Nichol, S. T., & Towner, J. S.
956 (2017). Egyptian rousette bats maintain long-term protective immunity against Marburg
957 virus infection despite diminished antibody levels. *Scientific Reports*, *7*(1), 1–7.

958 doi:10.1038/s41598-017-07824-2

959 Shi, J. J., Chan, L. M., Peel, A. J., Lai, R., Yoder, A. D., & Goodman, S. M. (2014). A deep
960 divergence time between sister species of *Eidolon* (Pteropodidae) with evidence for
961 widespread panmixia. *Acta Chiropterologica*, *16*(2), 279–292.
962 doi:10.3161/150811014X687242

963 Spangelo, B. L., Hall, N. R. S., Ross, P. C., & Goldstein, A. L. (1987). Stimulation of *in vivo*
964 antibody production and concanavalin-A-induced mouse spleen cell mitogenesis by
965 prolactin. *Immunopharmacology*, *14*(1), 11–20. doi:10.1016/0162-3109(87)90004-X

966 Swanepoel, R., Leman, P. A., Burt, F. J., Zachariades, N. A., Braack, L. E. O., Ksiazek, T.
967 G., … Peters, C. J. (1996). Experimental inoculation of plants and animals with Ebola
968 virus. *Emerging Infectious Diseases*, *2*(4), 321–325.

969 Taniguchi, S., Watanabe, S., Masangkay, J. S., Omatsu, T., Ikegami, T., Alviola, P., …
970 Morikawa, S. (1999). Reston ebolavirus antibodies in bats, the Philippines. *Emerging*
971 *Infectious Diseases*, *179 Suppl*(8), S115-9. doi:10.1086/514314

972 Trang, N. V, Choisy, M., Nakagomi, T., Chinh, N. T. M., Doan, Y. H., Yamashiro, T., …
973 Anh, D. D. (2015). Determination of cut-off cycle threshold values in routine RT-PCR
974 assays to assist differential diagnosis of norovirus in children hospitalized for acute
975 gastroenteritis. *Epidemiology and Infection*, *143*(15), 3292–9.
976 doi:10.1017/S095026881500059X

977 Wesolowski, A., Mensah, K., Brook, C. E., Andrianjafimasy, M., Winter, A., Buckee, C. O.,
978 … Metcalf, C. J. E. (2016). Introduction of rubella-containing-vaccine to Madagascar:
979 implications for roll-out and local elimination. *Journal of The Royal Society Interface*,
980 *13*(115), in press. doi:10.1098/rsif.2015.1101

981 Wilkinson, D. A., Mélade, J., Dietrich, M., Ramasindrazana, B., Soarimalala, V., Lagadec,

982 E., … Pascalis, H. (2014). Highly diverse Morbillivirus-related paramyxoviruses in the
983 wild fauna of southwestern Indian Ocean islands: Evidence of exchange between
984 introduced and endemic small mammals. *Journal of Virology*, (May).
985 doi:10.1128/JVI.01211-14
986 Wilkinson, D. A., Temmam, S., Lebarbenchon, C., Lagadec, E., Chotte, J., Guillebaud, J., …
987 Pascalis, H. (2012). Identification of novel paramyxoviruses in insectivorous bats of the
988 Southwest Indian Ocean. *Virus Research*, *170*(1–2), 159–63.
989 doi:10.1016/j.virusres.2012.08.022
990 Williams, B., Gouws, E., Wilkinson, D., & Karim, S. A. (2001). Estimating HIV incidence
991 rates from age prevalence data in epidemic situations. *Statistics in Medicine*, *20*, 2003–
992 2016. doi:10.1002/sim.840
993 Williamson, M. M., Hooper, P. T., Selleck, P. W., Gleeson, L. J., Daniels, P. W., Westbury,
994 H. A., & Murray, P. K. (1998). Transmission studies of Hendra virus (equine
995 morbillivirus) in fruit bats, horses and cats. *Aust Vet J*, *76*(12), 813–818.
996 doi:10.1111/j.1751-0813.1998.tb12335.x
997 Williamson, M. M., Hooper, P. T., Selleck, P. W., Westbury, H. A., & Slocombe, R. F.
998 (2000). Experimental Hendra virus infection in pregnant guinea-pigs and fruit bats
999 (*Pteropus poliocephalus*). *Journal of Comparative Pathology*, *122*(2–3), 201–207.
1000 doi:10.1053/jcpa.1999.0364
1001 Wood, S. N. (2001). mgcv: GAMs and Generalized Ridge Regression for R. *R News*, *1/2*,
1002 20–24.
1003 Yuan, J., Zhang, Y., Li, J., Zhang, Y., Wang, L.-F., & Shi, Z. (2012). Serological evidence of
1004 ebolavirus infection in bats, China. *Virology Journal*, *9*, 236. doi:10.1186/1743-422X-9-
1005 236

1006 Zhou, P., Tachedjian, M., Wynne, J. W., Boyd, V., Cui, J., Smith, I., … Baker, M. L. (2016).
1007 Contraction of the type I IFN locus and unusual constitutive expression of IFN-α in bats.
1008 *Proceedings of the National Academy of Sciences*, *113*(10), 2696–2701.
1009 doi:10.1073/pnas.1518240113
1010

Supporting Information

Text S1. Luminex Serological Assay.

In brief, recombinant HeV, NiV, CedV, EBOV, and MARV glycoproteins were conjugated to colored, distinguishable microspheres, to enable multiplexing. Antibody binding to each microsphere was detected after conjugation of bound antibodies with biotinylated Protein A and fluorescent streptavidin-R-phycoerythrin. Positive and negative controls included in each assay were from a range of wild species (*P. alecto* bats, monkeys, rabbits, and pigs), which have previously demonstrated extreme positive or negative values in microsphere and neutralization assays. Binding results were taken as the median fluorescence intensity (MFI) value of ≥100 microspheres for each virus; we report mean MFI values from two duplicate runs of each sample for each virus.

Text S2. Determining Serostatus: Finite Mixture Modeling

We used the R packages *MASS* (for a single normal distribution) and *mixtools* (for a mixture of two or three normal distributions) (Benaglia, Chauveau, Hunter, & Young, 2009) and fit each of twenty-four data subsets (eight antigens x three species) with mixtures of one, two, and three normal distributions in turn, then used likelihood ratio tests to select the best-fit model to the data (Table S1). In the case of a two-distribution model fit, we assumed log-MFI values in the lowest distribution to represent seronegative individuals and log-MFI values in the highest distribution to represent seropositive individuals. In the case of a three-distribution model fit, we assumed log-MFI values in both the lowest and middle distributions to represent seronegative individuals and log-MFI values in the highest distribution to represent seropositive individuals.

26
27
28 **Table S1. Fit comparison of normal distribution mixture models**

Bat species	Viral Antibody	# Fit Normal Distributions	Log-Likelihood	LRT†	P-Value‡
E. dupreanum	**EBOV-Gp**	1	-299.76	--	--
		2	**-258.19**	**83.15**	**0.000*****
		3	-258.17	0.03	0.987
	MARV-Gp	1	-85.10	--	--
		2	**-57.44**	**55.32**	**0.000*****
		3	-55.02	4.83	0.089
	CedV-F	1	-235.88	--	--
		2	-153.48	164.80	0.000***
		3	**-142.71**	**21.54**	**0.000*****
	CedPV-G	1	-294.53	--	--
		2	-235.86	117.34	0.000***
		3	**-230.29**	**11.14**	**0.004*****
	NiV-G	1	-635.13	--	--
		2	-578.31	113.64	0.000***
		3	**-566.26**	**24.10**	**0.000*****
	NiV-F	1	-558.74	--	--
		2	-522.36	72.75	0.000***
		3	**-515.67**	**13.39**	**0.001*****
	HeV-G	1	-500.41	--	--
		2	-426.23	148.36	0.000***
		3	**-422.18**	**8.10**	**0.017*****
	HeV-F	1	-619.01	--	--
		2	-592.09	53.84	0.000***
		3	**-584.87**	**14.45**	**0.001*****
P. rufus	**EBOV-Gp**	1	-292.04	--	--
		2	-267.38	49.32	0.000***
		3	**-263.65**	**7.45**	**0.024****
	MARV-Gp	1	-177.08	--	--
		2	**-137.46**	**79.26**	**0.000*****
		3	-135.09	4.72	0.094*
	CedV-F	1	-191.99	--	--
		2	-180.93	22.12	0.000***
		3	**-176.77**	**8.32**	**0.016****
	CedPv-G	1	-206.61	--	--
		2	-174.81	63.60	0.000***
		3	**-171.56**	**6.49**	**0.039****
	NiV-G	1	-220.35	--	--
		2	**-191.48**	**57.74**	**0.000*****
		3	-189.79	3.38	0.184
	NiV-F	1	-180.16	--	--
		2	**-162.23**	**35.87**	**0.000*****
		3	-159.29	5.87	0.053*
	HeV-G	1	-220.28	--	--
		2	**-200.64**	**39.29**	**0.000*****
		3	-198.25	4.77	0.092*
	HeV-F	1	-237.34	--	--
		2	-205.90	62.87	0.000***
		3	**-200.50**	**10.80**	**0.005*****
R. madagascariensis	**EBOV-Gp**	1	-385.06	--	--
		2	**-361.24**	**47.64**	**0.000*****

	3	-360.09	2.30	0.317
MARV-Gp	1	-343.05	--	--
	2	**-337.17**	**11.76**	**0.003*****
	3	-334.38	5.58	0.061*
CedV-F	1	-303.37	--	--
	2	**-272.31**	**62.11**	**0.000*****
	3	-272.09	0.44	0.804
CedPV-G	1	-294.04	--	--
	2	**-264.03**	**60.03**	**0.000*****
	3	-262.08	3.88	0.143
NiV-G	1	-261.81	--	--
	2	**-243.17**	**37.28**	**0.000*****
	3	-240.75	4.84	0.089*
NiV-F	1	-275.83	--	--
	2	-252.95	45.75	0.000***
	3	**-249.26**	**7.39**	**0.025****
HeV-G	1	-285.81	--	--
	2	**-258.78**	**54.06**	**0.000*****
	3	-257.27	3.02	0.221
HeV-F	1	-304.23	--	--
	2	**-288.16**	**32.13**	**0.000*****
	3	-286.38	3.57	0.168

Statistical significance by p-value standard <.1, <.05**, <.01*** . **We used a cutoff of .05 to determine the best-fit model to determine seroprevalence cutoffs (highlighted in bold).**
†Likelihood ratio test & ‡associated p-value from a chi-squared distribution comparing the binomial log-likelihood of the one to two or two to three distribution model mix via the following equation: 2*(ll(m2)-ll(m1)) where m1 = the model with fewer distributions.

We followed methods previously described in Burroughs et al., 2016 to select a cutoff MFI value for distinguishing between seropositive and seronegative samples in these distributions. For datasets best fit by two normal distributions, we selected a cutoff MFI value at four standard deviations above the mean value for the lower distribution (ensuring that 99.99+% of the MFI values encompassed in the lower distribution were classed as seronegative). For datasets best fit by three normal distributions, we selected a cutoff MFI value at three standard deviations above the mean value for the middle distribution (ensuring that 99.7% of values included in middle distribution were considered seronegative). We resampled our data 1000 times with replacement, refitting our best-fit mixture model with each resampling event, to generate a 95% confidence interval for our cutoff values at the seropositive thresholds (Table S2).

Table S2. Seroprevalence to henipa- and filovirus antigens in Madagascar fruit bats

Species	Virus	N	Viral Antigen Assayed	Max MFI	MFI Cutoff mean [lci*, uci**]	Seroprevalence % (N pos)		
						At mean cutoff	At lci cutoff*	At uci cutoff**
E. dupreanum	**Cedar***	**314**	**CedPV-G**	**2436.3**	**166.5 [95.7, 374.6]**	**0.64 (2)**	**1.27 (4)**	**0.64 (2)**
		263	CedV-F	430.5	63.2 [45.8, 97.1]	2.28 (6)	3.04 (8)	1.52 (4)
	Hendra/ Nipah†	**314**	**NiV-G**	**6553**	**402.9 [225.5, 1506.5]**	**24.2 (76)**	**32.17 (101)**	**10.19 (32)**
			HeV-G	1125.8	350.3 [153.0, 655.8]	5.73 (18)	13.38 (42)	2.23 (7)
			NiV-F	3542	1727.5 [510.7, 2568]	0.64 (2)	10.51 (33)	0.32 (1)
			HeV-F	5935.8	4774 [644.4, 7653]	0.64 (2)	24.84 (78)	0 (0)
	Ebola	314	EBOV-Gp	410.3	84.0 [79.6, 89.9]	2.87 (9)	3.18 (10)	2.87 (9)
	Marburg	314	MARV-Gp	67.5	28.4 [27.2, 29.5]	1.27 (4)	1.27 (4)	1.27 (4)
P. rufus	Cedar	201	CedPV-G	669.3	196.6 [94.9, 602.9]	1 (2)	1 (2)	0.5 (1)
		171	CedV-F	458	149.8 [84.8, 456.6]	1.75 (3)	2.34 (4)	0.50 (1)
	Hendra/ Nipah	**201**	NiV-G	383	51.0 [47.5, 58.2]	5.47 (11)	5.97 (12)	3.98 (8)
			HeV-G	**439.3**	**67.6 [61.3, 77.6]**	**5.47 (11)**	**6.97 (14)**	**3.48 (7)**
			NiV-F	287.8	84.9 [76.7, 93.8]	1 (2)	1 (2)	1 (2)
			HeV-F	372	88.1 [63.3, 161.8]	5.00 (10)	6.47 (13)	2.49 (5)
	Ebola†	**201**	**EBOV-Gp**	**697.5**	**110.5 [90.6, 284.0]**	**10.4 (21)**	**12.94 (26)**	**4.48 (9)**
	Marburg	201	MARV-Gp	155	34.4 [31.6, 36.4]	6.47 (13)	7.46 (15)	5.47 (11)
R. madagascariensis	**Cedar***	**225**	CedPV-G	1662.5	86.7 [77.7, 94.4]	4.44 (10)	5.33 (12)	4.44 (10)
			CedV-F	**623.8**	**75.8 [70.2, 84.0]**	**8.44 (19)**	**9.33 (21)**	**7.11 (16)**
	Hendra/ Nipah†	**225**	NiV-G	205.5	89.1 [81.7, 106.9]	4.44 (10)	4.89 (11)	4.44 (10)
			HeV-G	885.5	105.1 [96.6, 117.1]	5.78 (13)	5.78 (13)	4.89 (11)
			NiV-F	388.3	60.6 [32.3, 255.3]	6.67 (15)	15.56 (35)	1.33 (3)
			HeV-F	**437.3**	**77.5 [68.8, 94.8]**	**7.56 (17)**	**8.44 (19)**	**6.67 (15)**
	Ebola	**225**	**EBOV-Gp**	**5716**	**457.8 [358.5, 552.1]**	**8.44 (19)**	**12 (27)**	**6.67 (15)**
	Marburg	225	MARV-Gp	624.8	289.3 [195.8, 439.3]	4.44 (10)	8.89 (20)	1.33 (3)

All data subsets which met criteria for statistical analysis of seroprevalence trends are highlighted in **bold.** (Table 1 of the main text includes these bolded data only).
*lci = lower confidence interval threshold for the MFI cutoff for seropositivity. This is a more lenient threshold than the mean.
**uci = upper confidence interval threshold for the MFI cutoff for seropositivity. This is a stricter threshold than the mean.
†Of the seven subsets highlighted in **bold**, only two met more restrictive criteria for use in assessment of age-seroprevalence patterns. We report only results for NiV-G in *E. dupreanum* in the main text of the manuscript.

Our use of the normal distribution for mixture models fit to log-MFI data follows convention in the literature (Burroughs et al., 2016; Peel et al., 2013). One previous study found that data were better fit by a mixture model pairing a log-normal and Weibull distribution, though the change in cutoff MFI from the dual log-normal model was subtle

(Trang et al., 2015). Since we repeated all analyses using the lci and uci of the mean MFI, a range far exceeding any change wrought from an alternative distribution anyway, we felt justified in our use of the conventional dual log-normal distribution in our mixture models.

No data were fit best by a single normal distribution, which would have indicated an entirely seronegative distribution, or a complete failure of the assay to distinguish seropositivity in this system. We were nonetheless extremely cautious regarding the 13 data subsets fit best by a two distribution model due to large differences in the distributions' variances (seropositive distributions tended to have higher variance than seronegative distributions) and a large degree of overlap between distributions. Encouragingly, the mean of the seronegative distribution for all antigens was largely consistent within a given species though slightly higher than expected with *R. madagascariensis* anti-EBOV-Gp data (Fig. S1). We experimented with a variety of cutoff selection methods to discriminate between these distributions, following methods outlined in Hayman et al., 2008; Peel et al., 2013; and Trang et al., 2015 but, in an effort to minimize false positives, we ultimately adopted techniques outlined in Burroughs et al., 2016, which produced a more conservative estimate than was yielded by any other procedure. In the case of two distribution fits, we further enhanced the conservativeness of the cutoff procedure by one additional standard deviation.

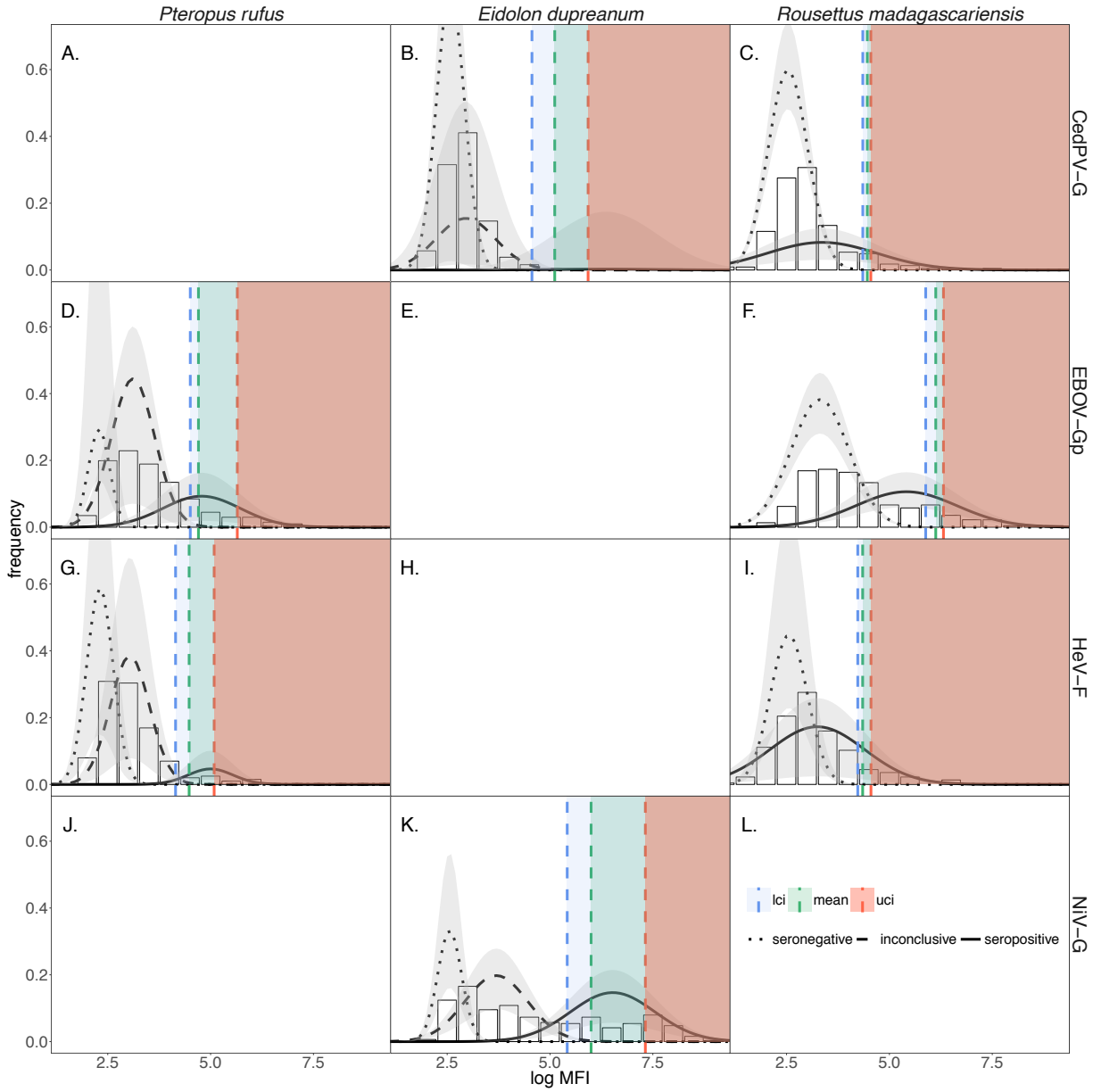

Fig. S1. ***Mixture model distributions and MFI cutoff values***
Best-fit finite mixture models (Table S1), fit to all seven species-serotype combinations that met our criteria for statistical analysis. The mean (green), lci (blue), and uci (red) MFI thresholds for seropositivity are shown as vertical dotted lines. Empty plots **(A, E, H, J, L)** represent those species-antigen combinations that did not meet our criteria for further analysis. Other plots depict species-antigen combinations for which seropositives were recovered: **(B)** CedPV-G in *E. dupreanum,* **(C)** CedV-G in *R. madagascariensis,* **(D)** EBOV-Gp in *P. rufus,* **(F)** EBOV-Gp in *R. madagascariensis,* **(G)** HeV-F in *P. rufus,* **(I)** HeV-F in *R. madagascariensis,* and **(K)** NiV-G in *E. dupreanum.*

We then identified each sample as seropositive or seronegative based on the calculated cutoff for each data subset and used the corresponding serostatus in all further prevalence-based analyses. Table 1 of the main text (and Table S2 here) gives the proportion of seropositive and seronegative individuals, and the corresponding MFI cutoffs, by antigen, by species. Seroprevalences obtained from the upper and lower confidence limits on the cutoff value are also included in these tables, and we report our results based on re-analysis of our data at these alternative thresholds throughout the manuscript. After cutoffs were calculated, data subsets were further assessed based on a strict set of acceptability criteria before being included in further ecological analyses (Text S3).

Text S3. Determining Serostatus: Criteria for Statistical Analysis

Because this assay was not originally designed for Madagascar samples, we required that each species-antigen-specific data subset meet several additional criteria to be considered acceptable for statistical analysis. As stated in the main text, for each data subset, we required that MFI values either (a) show correlation with an $R^2 > 40\%$ for associated soluble glycoproteins within the same viral genus (an indicator of reliable cross-reactivity among antibodies of related viruses), (b) have values > 1000 MFI for some individual[s] assayed (Gombos et al., 2013) and/or (c) result in > 10% seroprevalence based on the mixture model cutoff.

Only henipavirus antibodies were measurable by criterion (a), as this was the only viral genus for which multiple glycoproteins were assayed (HeV-G, NiV-G, HeV-F, NiV-F). In other systems, cross-reactive anti-henipavirus antibodies of the same soluble glycoprotein (either F or G) have yielded correlated MFI values in a given sample (Hayman et al., 2008). As such, we regressed HeV-G and NiV-G titers and HeV-F and NiV-F titers against one

105 another for samples derived from each of our three bat species (Fig. S2). Because all
106 correlations were significant, we selected the most reactive antibody of the pair yielding the
107 strongest correlation as our indicator of henipavirus serostatus per species and assumed that
108 we lacked the power to more definitively distinguish among Hendra/Nipah- related
109 henipavirus species. Differing antibody reactivities and correlation strengths across species
110 suggest that different henipaviruses could be infecting each of the three fruit bat species in
111 our system. All other seroptypes (EBOV-Gp, MARV-Gp, CedPV-G, or CedV-F) were
112 assessed by criteria (b) and/or (c) (Table 1, main text).
113

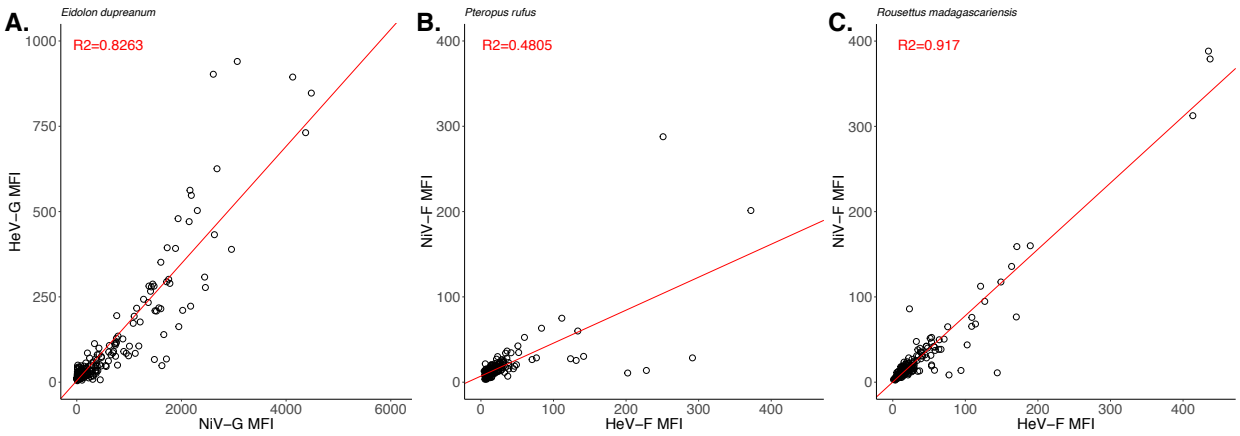

114
115
116
117 **Fig. S2.** ***Correlated MFI values for henipavirus serotypes.***
118 MFI values recovered for different species of henipavirus using antibodies to the same
119 soluble glycoprotein (i.e. NiV-G/HeV-G and NiV-F/HeV-F) were plotted against one
120 another, with a linear model (red line) fit to the resulting correlation. The strongest of these
121 paired correlations per species are shown here, with the most reactive antibody as the
122 independent variable: **(A)** NiV-G/HeV-G in *E. dupreanum,* **(B)** HeV-F/NiV-F in *P. rufus,*
123 and **(C)** HeV-F/NiV-F in *R. madagascariensis.* Such correlations are indicative of likely
124 antibody cross-reactivity from our samples against multiple known Hendra/Nipah-related
125 henipavirus antigens.
126
127

128 As stated in the main text of the manuscript, only seven species/antigen combinations
129 met classification criteria for further statistical analyses: NiV-G and CedPV-G in *E.*

130 *dupreanum*, HeV-F and EBOV-Gp in *P. rufus*, and HeV-F, CedPV-G, and EBOV-Gp in *R.*
131 *madagascariensis*. Once samples were characterized as seropositive/seronegative by all three
132 (mean, lower, upper) thresholds for seropositivity, we calculated the seroprevalence for each
133 of these species/antigen combinations across 42 discrete sampling events in our dataset
134 (Table S3). In conjunction with serological assay, a subset of *E. dupreanum* and *P. rufus*
135 individuals underwent aging via analysis of *cementum annuli.* For these bats, we further
136 calculated age-seroprevalence by sampling event, then compared age-seroprevalences with
137 the seroprevalence of the sampling event as a whole (which included unaged individuals). To
138 determine whether the aged subset was representative of the whole, we resampled all data
139 without replacement 1000 times from each sampling event that included aging, each time
140 randomly drawing a subsample the same size as that selected for aging in the actual study.
141 We then calculated the mean and standard deviation of these resampled subsamples and
142 classified real age-seroprevalence subsamples as representative if they fell within 1.5
143 standard deviations of the bootstrapped values (Table S3). For example, in sampling event
144 #17 (November 2013, Moramanga), we caught 46 *E. dupreanum* bats, fourteen of which
145 (30.4%) assayed seropositive to NiV-G. Within those 46 bats, thirteen underwent aging via
146 *cementum annuli* analysis of bat teeth. To assess the representativeness of our aged
147 subsample, we resampled our full sample of 46 bats (14 seropositive, 32 seronegative) 1000
148 times, randomly drawing a 13-bat sub-sample for aging each time. We then calculated the
149 mean (3.982) and standard deviation (1.45) of the number of seropositive bats (out of 13
150 possible) from these 1000 subsamples and determined that our actual subsample (4
151 seropositive bats) fell within 1.5 standard deviations of this mean, making it a representative
152 sub-sample justified for use in evaluation of fitted models. In the end, we opted to use only
153 the representative age-seroprevalence subsamples for NiV-G seroprevalence in *E.*

dupreanum and EBOV-Gp seroprevalence in *P. rufus* from our longitudinally-monitored Moramanga site in model-fitting analyses (Text S5, S6). Only one age-seroprevalence sub-sampling event (Event #29: April 2015 *E. dupreanum* in Moramanga) was discarded from our model-fitting based on these criteria: in this event, ten out of fifty bats (20%) assayed seropositive to NiV-G antigen in the broad survey, but none of the nine bats sub-sampled for aging were seropositive, yielding a non-representative 0% seroprevalence for that event.

Table S3: Seroprevalence by sampling event

Event	Site	Mid-Date	Species	Antigen	N	N-aged	Seroprevalence % (N pos)						
							Mean MFI cutoff	Mean cutoff *(aged)*	lci MFI cutoff	lci cutoff *(aged)*	uci MFI cutoff	uci cutoff *(aged)*	age fit? *
1	Moramanga	11/25/05	*E. dupreanum*	NiV-G	33	0	3 (1)	--	--	--	--	--	--
2	Moramanga	1/17/06	*E. dupreanum*	NiV-G	35	0	40 (14)	--	--	--	--	--	--
3	Moramanga	2/16/06	*E. dupreanum*	NiV-G	26	0	50 (13)	--	--	--	--	--	--
4	Moramanga	3/15/06	*E. dupreanum*	NiV-G	36	0	28 (10)	--	--	--	--	--	--
5	Moramanga	4/12/06	*E. dupreanum*	NiV-G	34	0	21 (7)	--	--	--	--	--	--
6	Moramanga	5/10/06	*E. dupreanum*	NiV-G	40	0	0 (0)	--	--	--	--	--	--
7	Moramanga	6/21/06	*E. dupreanum*	NiV-G	38	0	5 (2)	--	--	--	--	--	--
8	Moramanga	7/12/06	*E. dupreanum*	NiV-G	23	0	4 (1)	--	--	--	--	--	--
9	Moramanga	8/10/06	*E. dupreanum*	NiV-G	18	0	11 (2)	--	--	--	--	--	--
10	Moramanga	9/13/06	*E. dupreanum*	NiV-G	20	0	0 (0)	--	--	--	--	--	--
11	Moramanga	10/11/06	*E. dupreanum*	NiV-G	30	0	33 (10)	--	--	--	--	--	--
12	Moramanga	11/15/06	*E. dupreanum*	NiV-G	22	0	14 (3)	--	--	--	--	--	--
13	Moramanga	12/13/06	*E. dupreanum*	NiV-G	32	0	9 (3)	--	--	--	--	--	--
14	Moramanga	4/5/07	*E. dupreanum*	NiV-G	27	0	0 (0)	--	--	--	--	--	--
15	Moramanga	4/11/07	*E. dupreanum*	NiV-G	26	0	8 (2)	--	--	--	--	--	--
16	Moramanga	8/22/13	*E. dupreanum*	CedPV-G	5	0	0 (0)	--	0 (0)	--	0 (0)	--	--
16	Moramanga	8/22/13	*E. dupreanum*	NiV-G	5	0	60 (3)	--	60 (3)	--	40 (2)	--	--
17	Moramanga	11/19/13	*P. rufus*	EBOV-Gp	30	16	27 (8)	25 (4)	37 (11)	38 (6)	7 (2)	0 (0)	Y
17	Moramanga	11/19/13	*P. rufus*	HeV-F	30	16	3 (1)	0 (0)	3 (1)	0 (0)	0 (0)	0 (0)	--
17	Moramanga	11/26/13	*E. dupreanum*	CedPV-G	46	13	2 (1)	0 (0)	2 (1)	0 (0)	2 (1)	0 (0)	--
17	Moramanga	11/26/13	*E. dupreanum*	NiV-G	46	13	30 (14)	31 (4)	41 (19)	46 (6)	15 (7)	23 (3)	Y
18	Moramanga	2/22/14	*P. rufus*	EBOV-Gp	3	1	0 (0)	0 (0)	0 (0)	0 (0)	0 (0)	0 (0)	Y
18	Moramanga	2/22/14	*P. rufus*	HeV-F	3	1	0 (0)	0 (0)	0 (0)	0 (0)	0 (0)	0 (0)	--
19	Moramanga	3/20/14	*E. dupreanum*	CedPV-G	11	0	0 (0)	--	0 (0)	--	0 (0)	--	--
19	Moramanga	3/20/14	*E. dupreanum*	NiV-G	11	0	27 (3)	--	27 (3)	--	18 (2)	--	--
20	Mahabo	7/18/14	*E. dupreanum*	CedPV-G	14	8	0 (0)	0 (0)	0 (0)	0 (0)	0 (0)	0 (0)	--
20	Mahabo	7/18/14	*E. dupreanum*	NiV-G	14	8	7 (1)	0 (0)	21 (3)	12 (1)	0 (0)	0 (0)	--
20	Mahabo	7/19/14	*P. rufus*	EBOV-Gp	19	9	5 (1)	0 (0)	5 (1)	0 (0)	5 (1)	0 (0)	--
20	Mahabo	7/19/14	*P. rufus*	HeV-F	19	9	11 (2)	22 (2)	11 (2)	22 (2)	11 (2)	22 (2)	--
21	Ankarana	8/3/14	*E. dupreanum*	CedPV-G	27	6	0 (0)	0 (0)	0 (0)	0 (0)	0 (0)	0 (0)	--
21	Ankarana	8/3/14	*E. dupreanum*	NiV-G	27	6	4 (1)	0 (0)	11 (3)	0 (0)	4 (1)	0 (0)	--
21	Ankarana	8/3/14	*R. madagascariensis*	CedV-F	19	0	11 (2)	--	11 (2)	--	5 (1)	--	--
21	Ankarana	8/3/14	*R. madagascariensis*	EBOV-Gp	19	0	0 (0)	--	0 (0)	--	0 (0)	--	--
21	Ankarana	8/3/14	*R. madagascariensis*	HeV-F	19	0	5 (1)	--	5 (1)	--	5 (1)	--	--
22	Moramanga	9/12/14	*P. rufus*	EBOV-Gp	13	13	8 (1)	8 (1)	15 (2)	15 (2)	8 (1)	8 (1)	Y
22	Moramanga	9/12/14	*P. rufus*	HeV-F	13	13	0 (0)	0 (0)	0 (0)	0 (0)	0 (0)	0 (0)	--
23	Moramanga	10/4/14	*R. madagascariensis*	CedV-F	29	0	10 (3)	--	14 (4)	--	10 (3)	--	--
23	Moramanga	10/4/14	*R. madagascariensis*	EBOV-Gp	29	0	14 (4)	--	17 (5)	--	14 (4)	--	--
23	Moramanga	10/4/14	*R. madagascariensis*	HeV-F	29	0	3 (1)	--	7 (2)	--	3 (1)	--	--
23	Moramanga	10/8/14	*E. dupreanum*	CedPV-G	34	11	0 (0)	0 (0)	0 (0)	0 (0)	0 (0)	0 (0)	--
23	Moramanga	10/8/14	*E. dupreanum*	NiV-G	34	11	32 (11)	45 (5)	35 (12)	45 (5)	6 (2)	0 (0)	Y
24	Ankarana	10/15/14	*R. madagascariensis*	CedV-F	30	0	7 (2)	--	10 (3)	--	3 (1)	--	--
24	Ankarana	10/15/14	*R. madagascariensis*	EBOV-Gp	30	0	3 (1)	--	3 (1)	--	3 (1)	--	--
24	Ankarana	10/15/14	*R. madagascariensis*	HeV-F	30	0	3 (1)	--	7 (2)	--	3 (1)	--	--
24	Ankarana	10/18/14	*E. dupreanum*	CedPV-G	12	9	8 (1)	11 (1)	8 (1)	11 (1)	8 (1)	11 (1)	--
24	Ankarana	10/18/14	*E. dupreanum*	NiV-G	12	9	17 (2)	11 (1)	17 (2)	11 (1)	17 (2)	11 (1)	--

25	Makira	11/8/14	*P. rufus*	EBOV-Gp	3	3	0 (0)	0 (0)	0 (0)	0 (0)	0 (0)	0 (0)	--
25	Makira	11/8/14	*P. rufus*	HeV-F	3	3	0 (0)	0 (0)	33 (1)	33 (1)	0 (0)	0 (0)	--
25	Makira	11/9/14	*R. madagascariensis*	CedV-F	32	3	9 (3)	0 (0)	9 (3)	0 (0)	9 (3)	0 (0)	--
25	Makira	11/9/14	*R. madagascariensis*	EBOV-Gp	32	3	12 (4)	0 (0)	22 (7)	0 (0)	6 (2)	0 (0)	--
25	Makira	11/9/14	*R. madagascariensis*	HeV-F	32	3	12 (4)	0 (0)	12 (4)	0 (0)	9 (3)	0 (0)	--
26	Moramanga	12/9/14	*P. rufus*	EBOV-Gp	45	32	11 (5)	12 (4)	13 (6)	16 (5)	2 (1)	3 (1)	Y
26	Moramanga	12/9/14	*P. rufus*	HeV-F	45	32	11 (5)	16 (5)	16 (7)	19 (6)	7 (3)	9 (3)	--
26	Moramanga	12/13/14	*R. madagascariensis*	CedV-F	27	1	7 (2)	0 (0)	7 (2)	0 (0)	7 (2)	0 (0)	--
26	Moramanga	12/13/14	*R. madagascariensis*	EBOV-Gp	27	1	15 (4)	0 (0)	22 (6)	0 (0)	11 (3)	0 (0)	--
26	Moramanga	12/13/14	*R. madagascariensis*	HeV-F	27	1	4 (1)	0 (0)	4 (1)	0 (0)	4 (1)	0 (0)	--
26	Moramanga	12/18/14	*E. dupreanum*	CedPV-G	43	24	0 (0)	0 (0)	0 (0)	0 (0)	0 (0)	0 (0)	--
26	Moramanga	12/18/14	*E. dupreanum*	NiV-G	43	24	26 (11)	25 (6)	30 (13)	33 (8)	12 (5)	8 (2)	Y
27	Moramanga	3/22/15	*P. rufus*	EBOV-Gp	27	20	11 (3)	10 (2)	11 (3)	10 (2)	7 (2)	5 (1)	Y
27	Moramanga	3/22/15	*P. rufus*	HeV-F	27	20	0 (0)	0 (0)	0 (0)	0 (0)	0 (0)	0 (0)	--
28	Ankarana	3/31/15	*R. madagascariensis*	CedV-F	30	1	13 (4)	0 (0)	13 (4)	0 (0)	13 (4)	0 (0)	--
28	Ankarana	3/31/15	*R. madagascariensis*	EBOV-Gp	30	1	3 (1)	0 (0)	7 (2)	0 (0)	0 (0)	0 (0)	--
28	Ankarana	3/31/15	*R. madagascariensis*	HeV-F	30	1	13 (4)	0 (0)	13 (4)	0 (0)	13 (4)	0 (0)	--
28	Ankarana	4/2/15	*E. dupreanum*	CedPV-G	6	5	0 (0)	0 (0)	0 (0)	0 (0)	0 (0)	0 (0)	--
28	Ankarana	4/2/15	*E. dupreanum*	NiV-G	6	5	17 (1)	20 (1)	33 (2)	40 (2)	0 (0)	0 (0)	--
29	Moramanga	4/26/15	*R. madagascariensis*	CedV-F	30	2	3 (1)	0 (0)	3 (1)	0 (0)	0 (0)	0 (0)	--
29	Moramanga	4/26/15	*R. madagascariensis*	EBOV-Gp	30	2	3 (1)	0 (0)	7 (2)	0 (0)	3 (1)	0 (0)	--
29	Moramanga	4/26/15	*R. madagascariensis*	HeV-F	30	2	10 (3)	50 (1)	10 (3)	50 (1)	7 (2)	0 (0)	--
29	Moramanga	4/28/15	*E. dupreanum*	CedPV-G	50	9	0 (0)	0 (0)	2 (1)	0 (0)	0 (0)	0 (0)	--
29	Moramanga	4/28/15	*E. dupreanum*	NiV-G	50	9	20 (10)	0 (0)	26 (13)	0 (0)	10 (5)	0 (0)	--
30	Moramanga	5/19/15	*P. rufus*	EBOV-Gp	11	10	18 (2)	20 (2)	18 (2)	20 (2)	9 (1)	10 (1)	Y
30	Moramanga	5/19/15	*P. rufus*	HeV-F	11	10	0 (0)	0 (0)	0 (0)	0 (0)	0 (0)	0 (0)	--
31	Moramanga	6/21/15	*R. madagascariensis*	CedV-F	2	0	0 (0)	--	0 (0)	--	0 (0)	--	--
31	Moramanga	6/21/15	*R. madagascariensis*	EBOV-Gp	2	0	0 (0)	--	0 (0)	--	0 (0)	--	--
31	Moramanga	6/21/15	*R. madagascariensis*	HeV-F	2	0	0 (0)	--	0 (0)	--	0 (0)	--	--
31	Moramanga	6/24/15	*E. dupreanum*	CedPV-G	38	16	0 (0)	0 (0)	0 (0)	0 (0)	0 (0)	0 (0)	--
31	Moramanga	6/24/15	*E. dupreanum*	NiV-G	38	16	32 (12)	38 (6)	45 (17)	38 (6)	13 (5)	12 (2)	Y
32	Makira	7/16/15	*P. rufus*	EBOV-Gp	12	7	0 (0)	0 (0)	0 (0)	0 (0)	0 (0)	0 (0)	--
32	Makira	7/16/15	*P. rufus*	HeV-F	12	7	0 (0)	0 (0)	0 (0)	0 (0)	0 (0)	0 (0)	--
33	Moramanga	1/10/16	*E. dupreanum*	CedPV-G	28	8	0 (0)	0 (0)	4 (1)	12 (1)	0 (0)	0 (0)	--
33	Moramanga	1/10/16	*E. dupreanum*	NiV-G	28	8	25 (7)	25 (2)	39 (11)	38 (3)	4 (1)	12 (1)	Y
33	Moramanga	1/21/16	*P. rufus*	EBOV-Gp	38	31	3 (1)	3 (1)	3 (1)	3 (1)	3 (1)	3 (1)	Y
33	Moramanga	1/21/16	*P. rufus*	HeV-F	38	31	5 (2)	6 (2)	5 (2)	6 (2)	0 (0)	0 (0)	--
33	Moramanga	1/22/16	*R. madagascariensis*	CedV-F	26	0	8 (2)	--	8 (2)	--	8 (2)	--	--
33	Moramanga	1/22/16	*R. madagascariensis*	EBOV-Gp	26	0	15 (4)	--	15 (4)	--	15 (4)	--	--
33	Moramanga	1/22/16	*R. madagascariensis*	HeV-F	26	0	8 (2)	--	8 (2)	--	8 (2)	--	--

*For the purposes of mechanistic model fitting (Text S5, S6), we restricted our analysis to age-seroprevalence subsets from our one longitudinally re-sampled Moramanga site, as applied to NiV-G in *E. dupreanum* and EBOV-Gp in *P. rufus* (we additionally restricted reporting *P. rufus* EBOV-Gp results to the supplemental material, due to concerns over the lack of specificity in the assay). Within these parameters, we further assessed whether sub-sampled age-seroprevalence data from a given sampling event were representative of the age-seroprevalence of the sampling event as a whole by re-subsampling the broader sampling event 1000 times and calculating the mean and standard deviation of the resulting sub-samples. We included age-seroprevalence subsamples in fitting analyses if they fell within 1.5 standard deviations of the mean of the sub-sampled distribution.

178

179

180

181 *Text S4. GAMs for seasonality in seroprevalence and serostatus*

182 Using our longitudinal seroprevalence data (Table S3), we next used Generalized
183 Additive Models (GAMs) to assess the extent of seasonality in each antigen time series and
184 to explore-sex-specific patterns of seasonality within a given year. GAM structures took on
185 the basic forms listed below (all shown here for the *E. dupreanum* data subset though
186 structures were repeated for *P. rufus* and *R. madagascariensis* data as well). Outputs from
187 each GAM are summarized in the corresponding tables and figures below each formula.

188 *Text S4.a. Seroprevalence over time:*

189 The basic GAM structure took the following form:

190 Eid_CEDG <- gam(cbind(seropos, seroneg) ~ s(as.numeric(middat), k=7, bs="cr") + s(site,
191 bs="re"), family="binomial", data=seas.Eid)

192 Outputs for each species/antigen combination can be summarized as follows:
193
194

Table S4. Best fit GAMs by spp./antigen for seasonality in seroprevalence

Species	Viral Antigen	% Deviance explained	smoothing term	edf on smoother	chi-sq. value	p-value
E. dupreanum	CedPV-G	29.1	date	1	1.475	.225
			site	.241	.334	.236
	NiV-G (historical)	69.5	date	5.184	35.22	2.14×10^{-6}***
			site	--	--	--
	NiV-G (current)	66.2	date	1	.894	.3443
			site	1.356	9.278	.0014***
P. rufus	HeV-F	42.5	date	3.456	1.583	.815
			site	1.717×10^{-5}	0	.934
	EBOV-Gp	56.9	date	1	5.409	.020**
			site	.8446	1.655	.143
R. madagascariensis	CedV-F	99.5	date	4.81	2.559	.761
			site	0.00361	0	.300
	HeV-F	16.8	date	1.12	.693	.551
			site	0.0848	0.087	.339
	EBOV-Gp	75.7	date	2.783	3.739	.319
			site	.722	1.280	.159

195 *Statistical significance by p-value standard <.1*, <.05**, <.01***. Note that in figures (Fig. 1, main text; Fig.
196 S3, supplementary information) random effects of site are silenced for visualization purposes.

197

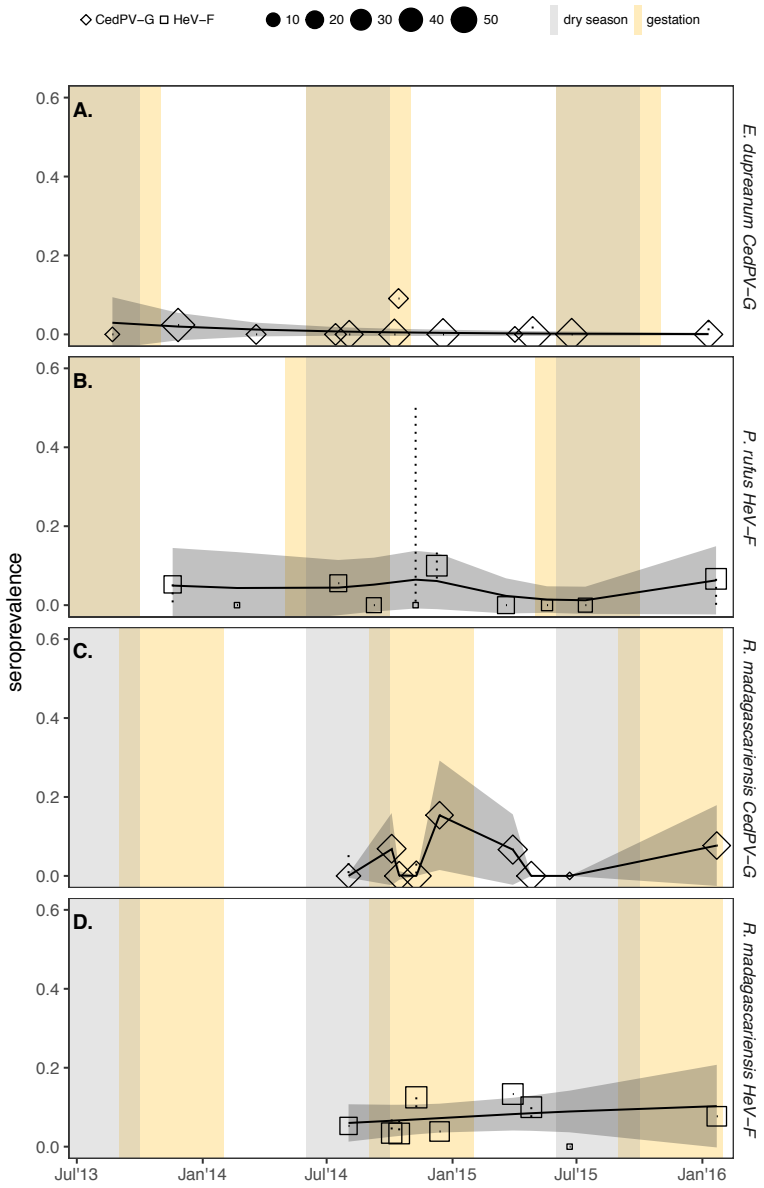

198
199
200 **Fig. S3.** ***Extensions to seasonality in seroprevalence.***
201 Plots are similar to those depicted in Fig. 1 (main text). **(A)** Predicted CedPV-G
202 seroprevalence by sampling date for *E. dupreanum,* across the date range of the authors' field
203 studies. Solid line and shaded 95% confidence intervals give the predictions from a
204 significant binomial GAM construction of seropositive vs. seronegative counts by sampling
205 date with random effects silenced for visualization purposes only. Data (with 95% exact
206 binomial confidence intervals) are shown as open shapes in the background; shape size is
207 correlated with sample size, as indicated in the legend. The nutrient-poor Madagascar dry
208 season is highlighted in gray vertical shading and the species-specific gestation period in
209 yellow. Analyses shown in **(B)**, **(C)**, **(D)** represent seroprevalence for HeV-F in *P. rufus,*
210 CedPV-G in *R. madagascariensis* and HeV-F in *R. madagascariensis,* respectively. GAM
211 constructions and results are summarized in Text S4 and Table S4. None of the seasonal
212 smoothers depicted here are significant.

Text S4.b. Serostatus within a year

The basic GAM structure took the following form:

```
E1prev <- gam(serostatus~  type + s(doy, by = sex, k=4, bs = "cc") + s(site, bs="re") +
            s(year, bs="re"), family="binomial", data=dat.Eid.prev)
```

Outputs for each species can be summarized as follows:

Table S5. Best fit GAM for seasonality in serostatus (family="binomial")

Fixed effects

Species	Term	MFI Cutoff	% Deviance explained	Estimate [lci – uci]	Z-stat	p-value*
E. dupreanum	Type: NiV-G	mean	48.2	3.87 [2.45-5.29]	5.35	9×10^{-8}***
		lci	66.4	3.56 [2.54-4.58]	6.86	6.97×10^{-12}***
		uci	35.6	2.74 [1.31-4.17]	3.71	.000206***
P. rufus	Type: HeV-F	mean	7.4	-.897 [-1.82 - .024]	-1.91	.0564*
		lci	7.98	-8.31 [-1.66 – .0021]	-1.96	.051**
		uci	3.9	-1.02 [-2.36 – .331]	-1.48	.139
R. madagascariensis	Type: EBOV-Gp	mean	11.3	.69 [-.102– 1.48]	1.71	.088*
		lci	11.4	.89 [.18 – 1.60]	2.46	.014*
		uci	9.89	.43 [-.39 – 1.26]	1.026	.305
	Type: HeV-F	mean	11.3	.57 [-.238 – 1.37]	1.38	.168
		lci	11.4	.49 [-.25 – 1.24]	1.30	.195
		uci	9.89	.43 [-.39 – 1.26]	1.026	.305

Smoothers

Species	Smoother	MFI cutoff	Ref.edf	Chi-Sq	P-value*
E. dupreanum	Day of Year (F)	mean	2	1784.35	.000893***
		lci	2	6.553	.0930*
		uci	2	.443	.254
	Day of Year (M)	mean	2	3.459	617
		lci	2	0	.808
		uci	2	0	.536
	Site	mean	4	27.026	.0675*
		lci	4	2.94	.1524
		uci	4	0	.364
	Year	mean	6	23.402	.0377**
		lci	3	5.234	.0158**
		uci	3	2.92	.112
P. rufus	Day of Year (F)	mean	2	0	.389
		lci	2	0.089	.295
		uci	2	0	1

	Day of Year (M)	mean	2	0	.665
		lci	2	0	.768
		uci	2	0	.798
	Site	mean	3	0	.436
		lci	3	0	.520
		uci	3	0	.481
	Year	mean	3	3.19	.123
		lci	3	5.05	.0581*
		uci	3	0	.663
R. madagascariensis	Day of Year (F)	mean	2	6.09	.0236**
		lci	2	3.091	.096*
		uci	2	5.71	.029**
	Day of Year (M)	mean	2	0	.591
		lci	2	0	.620
		uci	2	0	.662
	Site	mean	2	0	.335
		lci	2	1.285	.181
		uci	2	.142	.274
	Year	mean	2	0	.913
		lci	2	0	.656
		uci	2	0	.952

Statistical significance by p-value standard <.1, <.05**, <.01***

Results are visualized in Fig. 2A-C of the main text (females only) and in Fig. S4 (males).

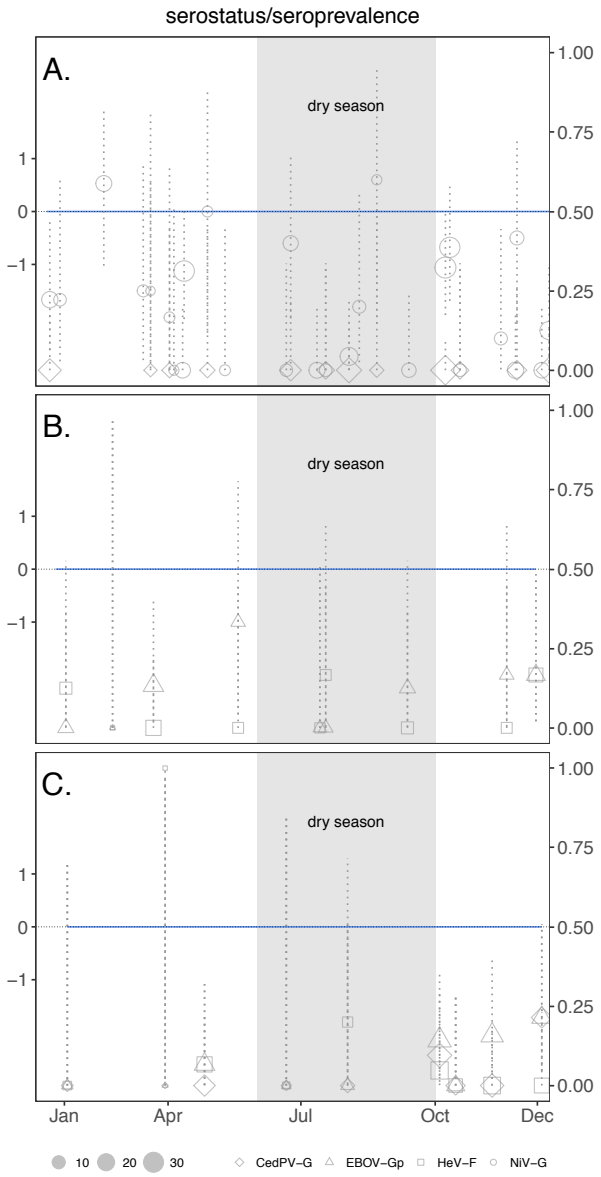

Fig. S4. ***Lack of seasonality in serostatus for male fruit bats***
Seasonal serostatus in male (**A**) *E. dupreanum,* (**B**) *P. rufus,* and (**C**) *R. madagascariensis.* The nutrient-poor Madagascar dry season is highlighted in gray shading. Solid blue lines show the [flat] cyclical smoothing spline (*k*=4*)* from day of year smoother for the binomial GAM with serostatus as the response variable (left y-axis). Data for raw seroprevalence per sampling event (with 95% exact binomial confidence intervals) are shown as open shapes in the background (right y-axis; shape type corresponds to antigen, as indicated in legend). Note that *E. dupreanum* data are combined with 2005-2007 sampling data from IPM. Full GAM constructions are reported in Text S4 and results summarized in Table S5.

235 Recapture data were too scarce for any meaningful statistical analysis, but we nonetheless
236 plotted Nipah virus MFI titers for recaptured *E. dupreanum*. Four of the bats (3M, 1F)
237 demonstrated dynamic titers which waxed or waned across the time series of the study.
238
239

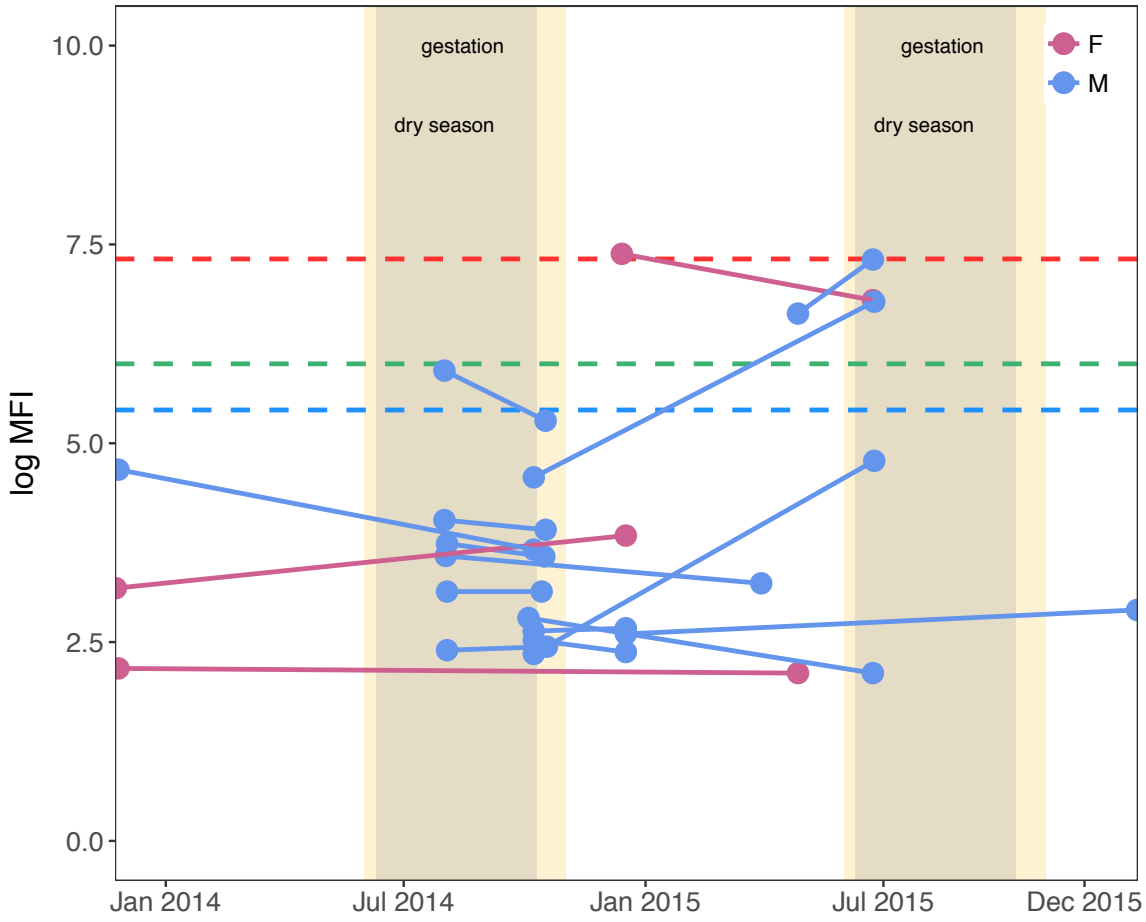

240
241
242 **Fig. S5. *Recaptured* E. dupreanum *individuals***
243 We captured seventeen individual *E. dupreanum* (14 M, 3 F) twice across the duration of our
244 time series. Each line segment connects the two anti-NiV-G MFI values (log scale) for a
245 distinct individual, with respect to date of sampling. We overlay these values on a time series
246 highlighting the periodicity of *E. dupreanum* gestation (yellow) and of Madagascar's
247 nutrient-poor dry season (gray).
248
249
250

Text S4.c. Mass:forearm residual within a year

The basic GAM structure took the following form:

```
E1 <- gam(mass_forearm_residual ~  s(doy, by = sex, k=4, bs = "cc") +
        s(site, bs="re") + s(year, bs="re"), family="gaussian", data=dat.Eid)
```

Outputs for each species can be summarized as follows:

Table S6. Best fit GAM for seasonality in body condition (family = "Gaussian")

Species	% Deviance explained	Smoothing Term	edf	F-stat	P-value*
E. dupreanum	19.3%	Day of Year (F)	2	18.33	3.77e-7***
		Day of Year (M)	2	2.47	.308
		Site	4	36.87	<2e-16***
		Year	1	2.97	7.35e-10***
P. rufus	21.7%	Day of Year (F)	2	2.42	.070*
		Day of Year (M)	2	5.17	.00385**
		Site	3	7.88	1.8e-5***
		Year	1	0	.822
R. madagascariensis	24.3%	Day of Year (F)	2	2.77	.042**
		Day of Year (M)	2	2.12	.042*
		Site	2	20.43	1.66e-10***
		Year	1	.013	.0022*

Statistical significance by p-value standard <.1, <.05**, <.01***

GAM outputs are summarized in Fig. 2D-F (males) and Fig. 2G-I (females of the main text). Mass:forearm residuals were calculated as the residual of each datapoint from the standard major axis type 2 linear regression visualized on the following page (Fig. S6).

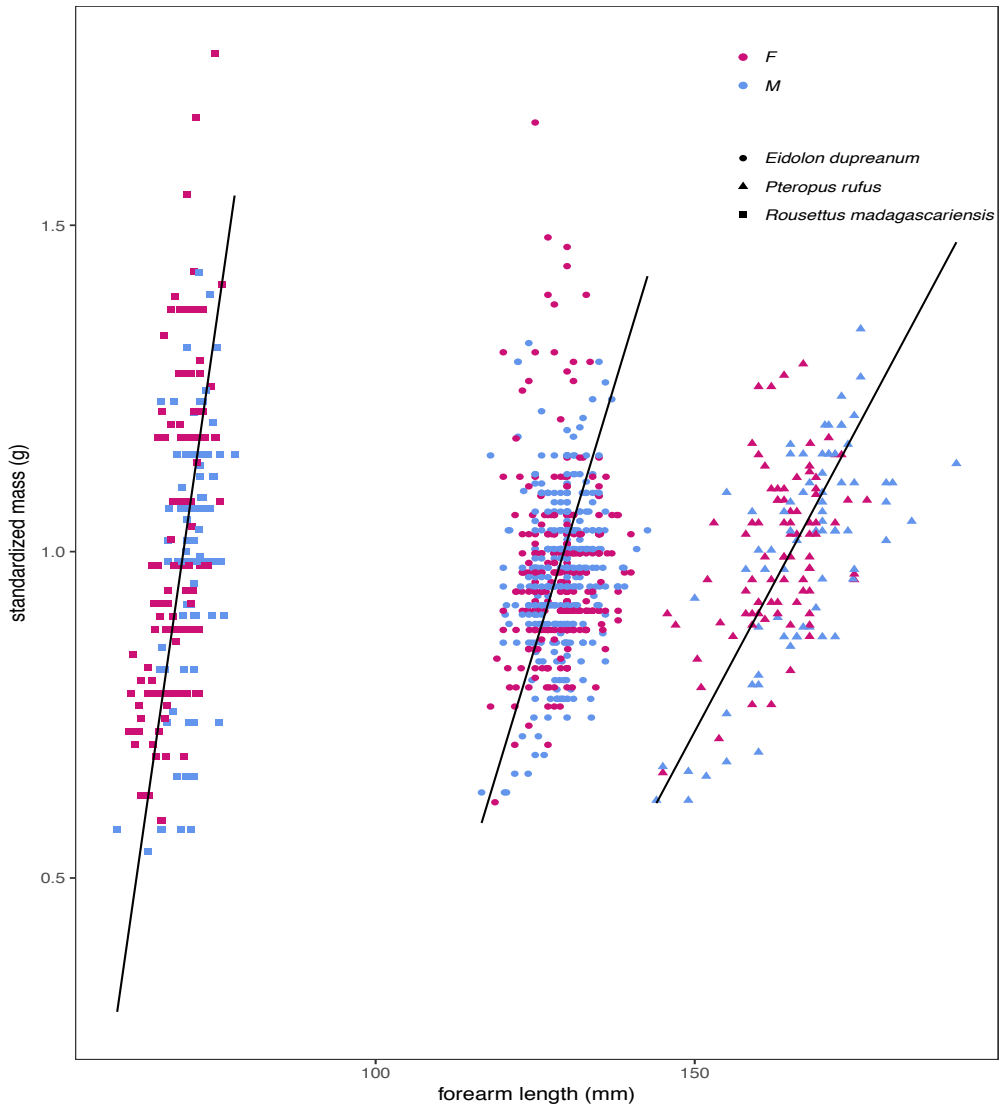

Fig. S6. ***Mass: forearm trends by species***
Forearm length in mm (x-axis) predicts standardized body mass (y-axis) for adult bats of all three species (circles = *E. dupreanum;* triangles = *P. rufus;* squares=*R. madagascariensis*). Standardized mass was computed by dividing the mass of each adult bat in the dataset by the mean mass of that particular species and sex (pink=females; blue=males). A separate linear model (via "standard major axis" type 2 linear regression) was fit to each species-specific subset of the data, and residuals from the fitted line were used as a measure of nutritional condition for each individual.

Text S5: Mechanistic models and age-seroprevalence data

In order to recover the mechanistic drivers of age-seroprevalence patterns in our data, we first examined age-structured patterns in our Luminex data, with an eye towards establishing definitive disease state classes. Firstly, we observed that simultaneously captured and sampled dam-pup pairs of both *E. dupreanum* and *P. rufus* demonstrated tightly correlated MFI titers for all seropositive antigens, an indication that maternally-inherited antibodies play a role in transmission dynamics in this system:

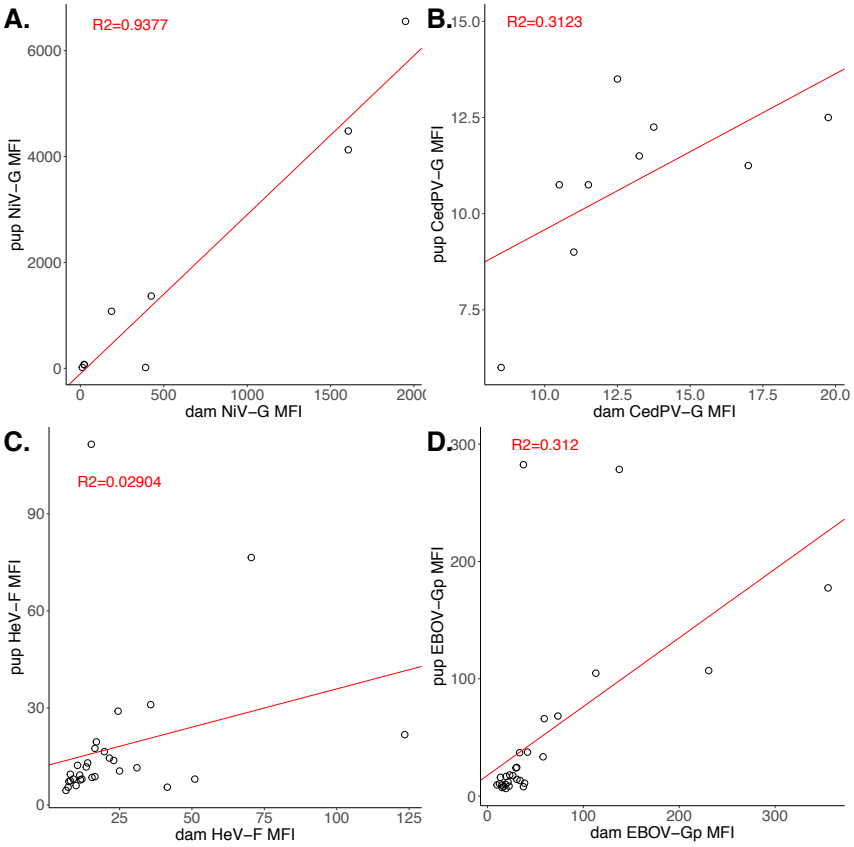

Fig. S7. *Dam-pup titer correlations in* E. dupreanum *and* P. rufus.
Correlated MFI values for dam-pup pairs in Luminex assay, using all *E. dupreanum/P. rufus* serotypes which met our criteria for seroprevalence analysis. Open circles = data (each point represents one dam-pup pair); red line= projections from fitted linear model: **(A)** anti-NiV-G antibodies in *E. dupreanum* (R^2 =.9377), **(B)** anti-CedPV-G values in *E. dupreanum* (R^2 =.3123), **(C)** anti-HeV-F antibodies in *P. rufus* (R^2 =.0290), **(D)** anti-EBOV-Gp antibodies in *P. rufus* (R^2 =.3120).

We then combined serological data amassed under Aim 1 with age information from fruit bat teeth (Fig. 3, main text) to construct age-seroprevalence curves for *E. dupreanum* NiV-G and *P. rufus* EBOV-Gp. Because we collected these data longitudinally, we were able to visualize the temporal age-seroprevalence patterns for both species-antigen combination across the year at each discrete sampling event, as summarized in Table S3 and Figs S8, S9:

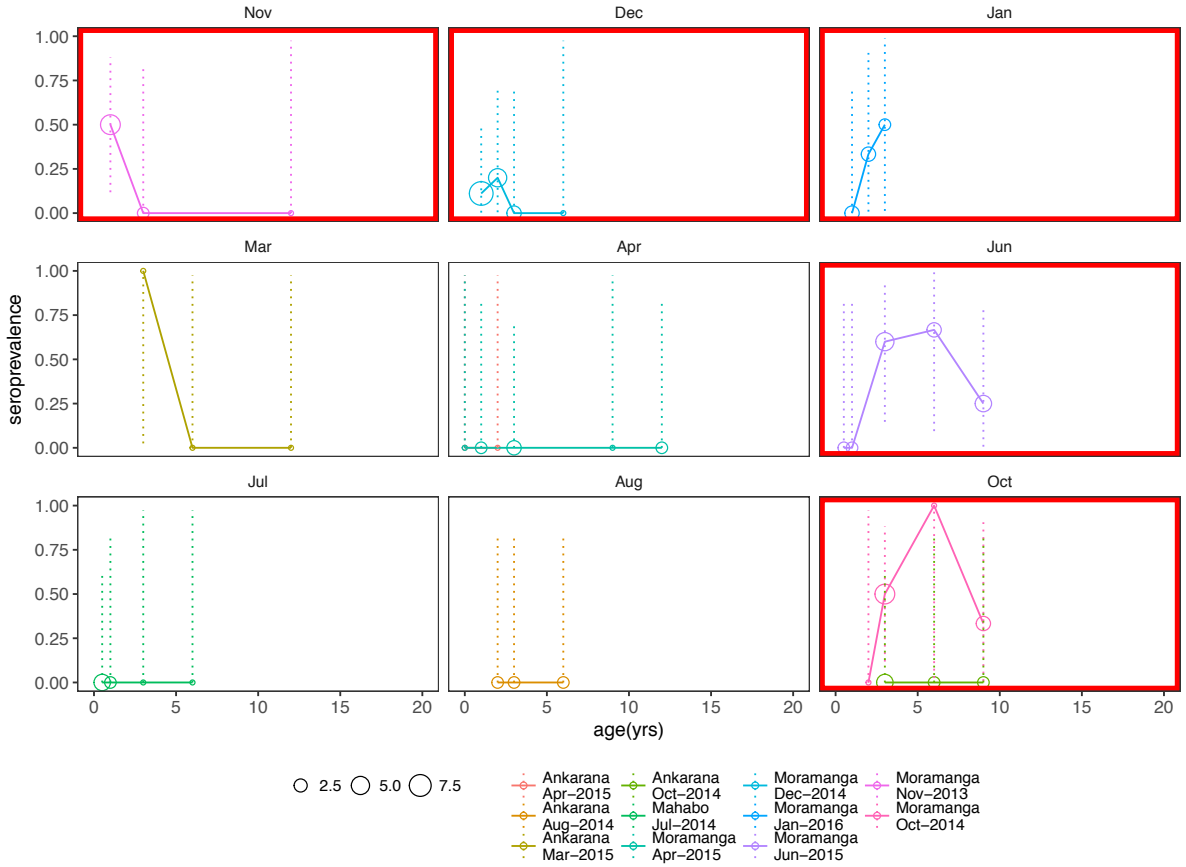

Fig. S8. ***Temporal age-seroprevalence for*** **E. dupreanum** ***NiV-G***
Age-seroprevalence data, assuming the mean MFI cutoff for seropositivity for NiV-G in *E. dupreanum,* are shown as separately colored lines/circles (with a 95% binomial confidence interval), stratified by sampling location and time, as indicated in the legend. Circle size corresponds to sampling size, as also indicated in the legend. Data are organized by month of the year in which they were collected, beginning Nov 1, the modeled annual birth date for *E. dupreanum* (though note that our models allow a normal distribution of births within 5 biweeks on either side of this date). Plots bordered in red indicate data from the longitudinally-resampled Moramanga sites, to which all dynamical models were fit (April 2015 was discarded from fitting after being determined an unrepresentative sub-sample; see Text S3, Table S3).

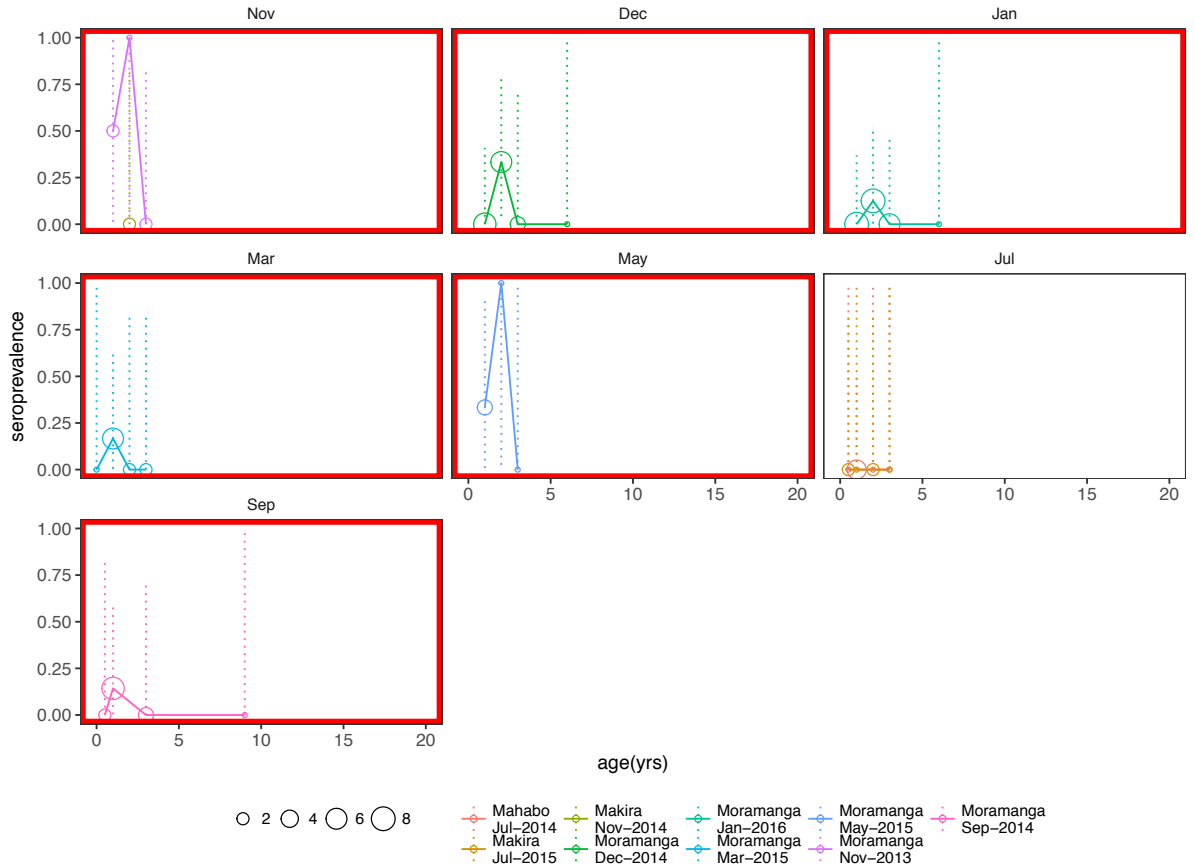

Fig. S9. ***Temporal age-seroprevalence for*** **P. rufus** ***EBOV-Gp***
Figure is similar to that depicted in Fig. S8 but shows age-seroprevalence data, assuming the mean MFI cutoff for seropositivity, for EBOV-Gp in *P. rufus.* Data are depicted as separately colored lines/circles (with a 95% binomial confidence interval), stratified by sampling location and time, as indicated in the legend. Circle size corresponds to sampling size, as also indicated in the legend. Data are organized by month of the year in which they were collected, beginning Oct 1, the modeled annual birth date for *P. rufus* (though note that our models allow a normal distribution of births within 5 biweeks on either side of this date). Plots bordered in red indicate data from the longitudinally-resampled Moramanga sites, to which all dynamical models were fit.

Ultimately, we aimed to fit a series of epidemiological models, representing a suite of transmission hypotheses in bat viral dynamics, to the time-course of age-seroprevalence for NiV-G in *E. dupreanum* and EBOV-Gp in *P. rufus* data, in order to elucidate the mechanisms underpinning observed patterns in the data. Model outputs are visualized over the composite age-seroprevalence data summarized across one calendar year in Fig. 4 for *E. dupreanum* (main text) and in Fig. S10 for *P. rufus* (below). All models were refit to age-seroprevalence

data recalculated using both the lower and upper MFI thresholds for seropositivity. Results were robust to the full range of cutoff thresholds (Fig. S11-12) and patterns and inferences largely consistent across both *E. dupreanum* NiV-G and *P. rufus* EBOV-Gp data.

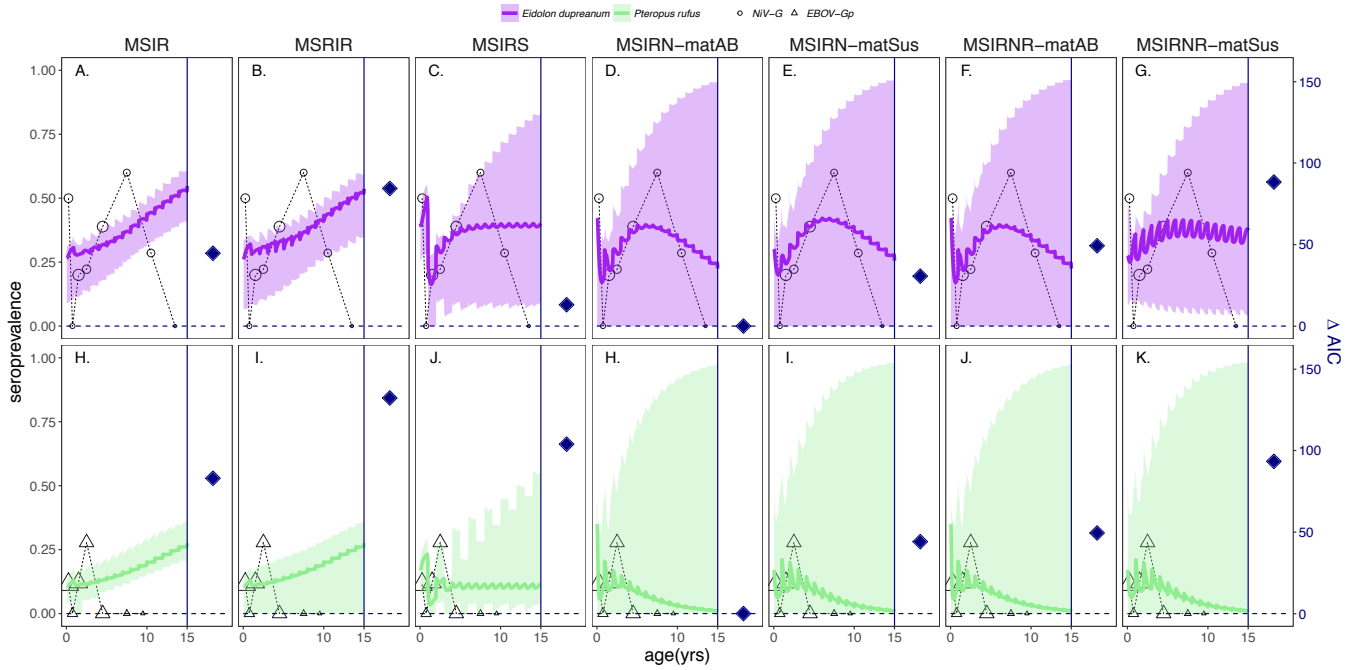

Fig. S10. *Expanded Model fits to age-seroprevalence data using mean MFI cutoffs, for , EBOV-Gp in* P. rufus

Age-seroprevalence curves for *E. dupreanum* NiV-G (A-G) and *P. rufus* EBOV-Gp (H-K), using the mean MFI cutoff for seropositive status. Seroprevalence data (left y-axis) are shown as open circles, binned for 0-.5 yrs, .5-1 yrs, 1-1.5yrs, 1.5-3 yrs, and for 3-yr increments increasing after that. Shape size corresponds to the number of bats sampled per bin (respective sample sizes, by age bin, are for *E. dupreanum*: N= 10,2,20,9,18,5,7,1 and for *P. rufus*: N=44,7,33,18,18,2,1). Solid lines indicate model outputs, and translucent shading highlights the 95% confidence interval derived from the Hessian matrix of the maximum likelihood of each model fit to the data (purple = *E. dupreanum;* green = *P. rufus*). Panels are stratified into columns by model structure: **(A/H)** MSIR = Maternally immune, Susceptible, Infectious, Recovered; **(B/I)** MSRIR= Maternally immune, Susceptible, Recovered via direct seroconversion, Infectious, Recovered; **(C/J)** MSIRS = Maternally immune, Susceptible, Infectious, Recovered, Susceptible; **(D/H)** MSIRN-matAB= Maternally immune, Susceptible, Infectious, Recovered, Non-antibody immune; **(E/I)** MSIRN-matSus= Maternally immune, Susceptible, Infectious, Recovered, Non-antibody immune; **(F/J)** MSIRNR-matAB = Maternally immune, Susceptible, Infectious, Recovered, Non-antibody immune; Recovered); **(G/K)** MSIRNR-matSus = Maternally immune, Susceptible, Infectious, Recovered, Non-antibody immune; Recovered). Note that MSIRN/R-matAB models assume that Non-antibody immune dams produce Maternally immune-class young, while MSIRN/R-matSus models assumer that Non-antibody immune dams produce Susceptible young. The right-hand y-axis (in navy) of each subplot shows ΔAIC for each model fit, relative to all other models for that species/antigen combination (navy diamonds). The MSIRN-matAB model (D/H) offered the best fit to the data, corresponding to ΔAIC = 0.

All parameter values, confidence intervals, and raw AIC scores for each model fit are reported in Table S7. Model fits to seroprevalence data calculated using the lower and upper MFI thresholds for seropositivity are shown in Fig. S11-12.

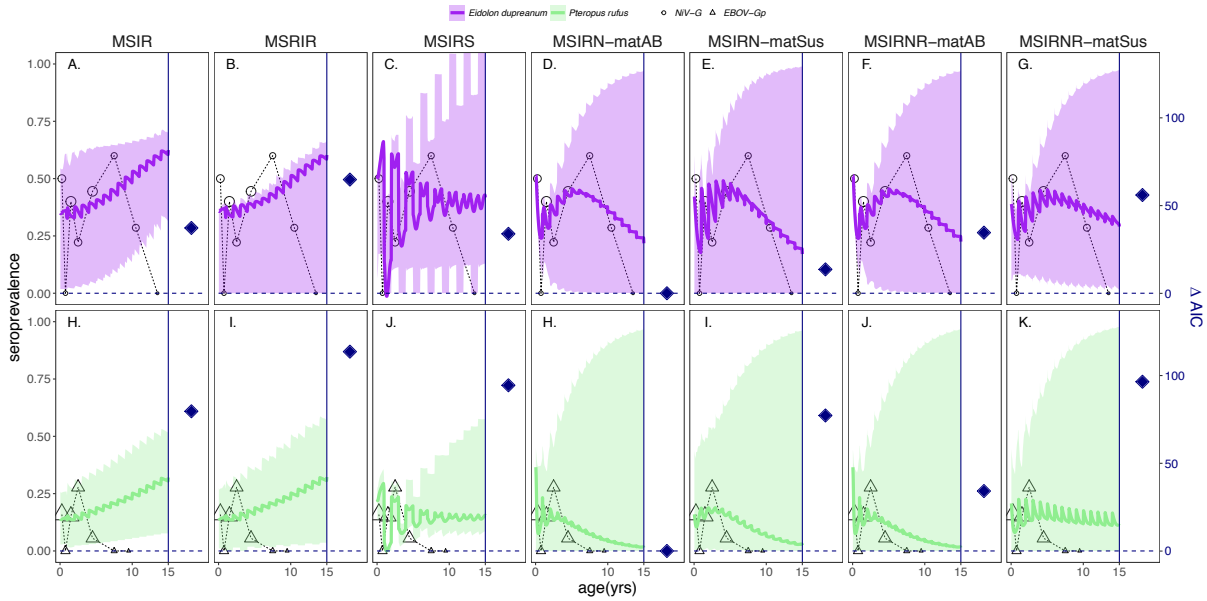

Fig. S11. ***Model fits to age-seroprevalence data, using the lower threshold MFI cutoff for seropositivity***

Figure is the same as that depicted in Fig. S10 but, here, age-seroprevalence is calculated using the lower threshold (most lenient) MFI cutoff for seropositivity. Models fits to the data are shown as solid colored lines (purple = *E. dupreanum;* green= *P. rufus*), with the 95% confidence intervals in the translucent shaded background. ΔAIC for models of each species-specific row compared against one another are shown in the right-hand subpanel of each plot (navy triangles), corresponding to the right y-axis; as with the mean MFI cutoff (S10), the MSIRN-matAB model offered the best fit in all cases. All parameter values, confidence intervals, and raw AIC scores for each model fit are reported in Table S7.

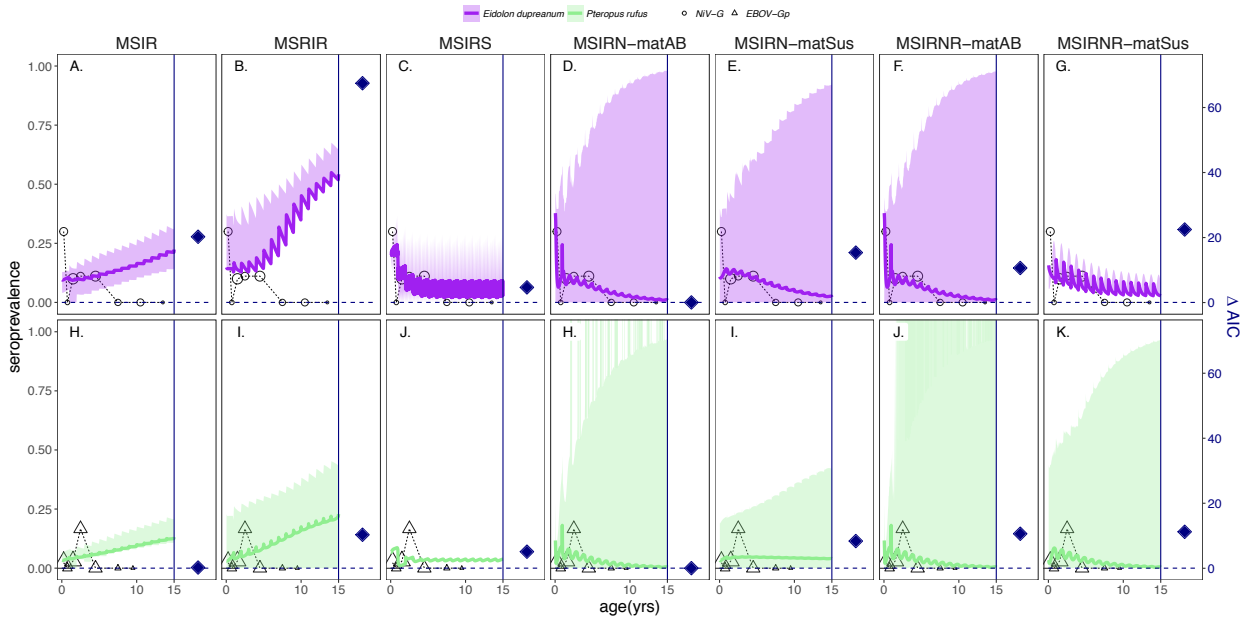

Fig. S12. ***Model fits to age-seroprevalence data, using the upper threshold MFI cutoff for seropositivity***
Figure is the same as that depicted in Fig. S10 and S11 but, here, age-seroprevalence is calculated using the upper threshold (most strict) MFI cutoff for seropositivity. Models fits to the data are shown as solid colored lines (purple = *E. dupreanum;* green= *P. rufus*), with the 95% confidence intervals in the translucent shaded background. ΔAIC for models of each species-specific row compared against one another are shown in the right-hand subpanel of each plot (navy triangles), corresponding to the right y-axis; as with the mean MFI cutoff (S10), the MSIRN-matAB model offered the best fit in all cases. All parameter values, confidence intervals, and raw AIC scores for each model fit are reported in Table S7.

In the end, we chose to report model fits for the *E. dupreanum* NiV-G data only in the main text of the manuscript and restricted the *P. rufus* EBOV-Gp data to this Supporting Information due to concerns over the lack of specificity and validation in our serological assay. *P. rufus* samples challenged with the Zaire ebolavirus antigen (EBOV-Gp) reached a high maximum MFI value of 697.5 and a corresponding seroprevalence of 10.4%, based on a mean, mixture-model-calculated MFI cutoff of 110.5 (Table 1, S2). These findings strongly suggest that antibodies in *P. rufus* serum are, indeed, binding Zaire ebolavirus antigen non-randomly in our assay, but the resulting seroprevalances, even at the most lenient MFI cutoff, were low, offering little power for dynamical model fitting. We hope that increased

407 sampling, especially across a longitudinal gradient, will improve our capacity for inference in
408 the future.

409 To simulate our age-structured epidemics, we first constructed a simple demographic
410 Leslie matrix, allowing bats to occupy annual age classes from one to twenty (Leslie, 1945,
411 1948). To obtain estimates for annual adult survival, we fit an exponential model to the age-
412 frequency distribution recovered from *cementum annuli* analysis of bat teeth for bats over six
413 months in age (Fig. 3, main text), following techniques adopted in Hayman et al., 2012. We
414 recovered an annual adult survival rate of .793 for *E. dupreanum* and .511 for *P. rufus.* For
415 both species, we adopted an estimate of adult fecundity of .48, equivalent to that reported for
416 *E. helvum* in Ghana Hayman et al., 2012 (we modeled only females), and we allowed bats to
417 begin reproduction at the end of the second year of life. Our models assumed a post-breeding
418 census.

419 For the purposes of epidemic modeling, we assumed equilibrium population
420 dynamics and assigned juvenile survival at the rate needed to maintain stable population size
421 and age structure for *E. dupreanum* (where λ, the dominant eigenvalue of the demographic
422 transition matrix equals one): .544. Such an assumption was impossible in the case of *P.*
423 *rufus,* since adult survival was too low to be effectively counterbalanced by higher juvenile
424 survival. Therefore, we simply fixed the annual juvenile survival rate for *P. rufus* at the same
425 magnitude as that recovered for *E. dupreanum* (.544) but kept adult annual survival at our
426 tooth-estimated value for *P. rufus* (.511), such that the overall population size was in decline
427 but equilibrium structure was maintained across age classes. It should be noted that adult
428 annual survival estimates for *P. rufus* suggest that the species may be in serious population
429 decline and a cause for conservation concern.

Our basic demographic matrix thus took on the following form for *E. dupreanum* (values of .793 were simply replaced with .511 for *P. rufus*):

$$\begin{bmatrix}
0 & .381 \\
.544 & 0 & 0 & 0 & 0 & 0 & 0 & 0 & 0 & 0 & 0 & 0 & 0 & 0 & 0 & 0 & 0 & 0 & 0 & 0 & 0 \\
0 & .793 & 0 & 0 & 0 & 0 & 0 & 0 & 0 & 0 & 0 & 0 & 0 & 0 & 0 & 0 & 0 & 0 & 0 & 0 & 0 \\
0 & 0 & .793 & 0 & 0 & 0 & 0 & 0 & 0 & 0 & 0 & 0 & 0 & 0 & 0 & 0 & 0 & 0 & 0 & 0 & 0 \\
0 & 0 & 0 & .793 & 0 & 0 & 0 & 0 & 0 & 0 & 0 & 0 & 0 & 0 & 0 & 0 & 0 & 0 & 0 & 0 & 0 \\
0 & 0 & 0 & 0 & .793 & 0 & 0 & 0 & 0 & 0 & 0 & 0 & 0 & 0 & 0 & 0 & 0 & 0 & 0 & 0 & 0 \\
0 & 0 & 0 & 0 & 0 & .793 & 0 & 0 & 0 & 0 & 0 & 0 & 0 & 0 & 0 & 0 & 0 & 0 & 0 & 0 & 0 \\
0 & 0 & 0 & 0 & 0 & 0 & .793 & 0 & 0 & 0 & 0 & 0 & 0 & 0 & 0 & 0 & 0 & 0 & 0 & 0 & 0 \\
0 & 0 & 0 & 0 & 0 & 0 & 0 & .793 & 0 & 0 & 0 & 0 & 0 & 0 & 0 & 0 & 0 & 0 & 0 & 0 & 0 \\
0 & 0 & 0 & 0 & 0 & 0 & 0 & 0 & .793 & 0 & 0 & 0 & 0 & 0 & 0 & 0 & 0 & 0 & 0 & 0 & 0 \\
0 & 0 & 0 & 0 & 0 & 0 & 0 & 0 & 0 & .793 & 0 & 0 & 0 & 0 & 0 & 0 & 0 & 0 & 0 & 0 & 0 \\
0 & 0 & 0 & 0 & 0 & 0 & 0 & 0 & 0 & 0 & .793 & 0 & 0 & 0 & 0 & 0 & 0 & 0 & 0 & 0 & 0 \\
0 & 0 & 0 & 0 & 0 & 0 & 0 & 0 & 0 & 0 & 0 & .793 & 0 & 0 & 0 & 0 & 0 & 0 & 0 & 0 & 0 \\
0 & 0 & 0 & 0 & 0 & 0 & 0 & 0 & 0 & 0 & 0 & 0 & .793 & 0 & 0 & 0 & 0 & 0 & 0 & 0 & 0 \\
0 & 0 & 0 & 0 & 0 & 0 & 0 & 0 & 0 & 0 & 0 & 0 & 0 & .793 & 0 & 0 & 0 & 0 & 0 & 0 & 0 \\
0 & 0 & 0 & 0 & 0 & 0 & 0 & 0 & 0 & 0 & 0 & 0 & 0 & 0 & .793 & 0 & 0 & 0 & 0 & 0 & 0 \\
0 & 0 & 0 & 0 & 0 & 0 & 0 & 0 & 0 & 0 & 0 & 0 & 0 & 0 & 0 & .793 & 0 & 0 & 0 & 0 & 0 \\
0 & 0 & 0 & 0 & 0 & 0 & 0 & 0 & 0 & 0 & 0 & 0 & 0 & 0 & 0 & 0 & .793 & 0 & 0 & 0 & 0 \\
0 & 0 & 0 & 0 & 0 & 0 & 0 & 0 & 0 & 0 & 0 & 0 & 0 & 0 & 0 & 0 & 0 & .793 & 0 & 0 & 0 \\
0 & 0 & 0 & 0 & 0 & 0 & 0 & 0 & 0 & 0 & 0 & 0 & 0 & 0 & 0 & 0 & 0 & 0 & .793 & 0 & 0 \\
0 & 0 & 0 & 0 & 0 & 0 & 0 & 0 & 0 & 0 & 0 & 0 & 0 & 0 & 0 & 0 & 0 & 0 & 0 & .793 & .793
\end{bmatrix}$$

For the purposes of epidemic modeling, we recovered the stable-age distribution as the dominant eigenvector of the above matrix and assigned a base population of 10000 simulated bats by age class according to these proportions. Following Klepac and Caswell 2011 (Klepac & Caswell, 2011), we replicated our population vector according to the number of epidemic states in the model under consideration (four times for MSIR/MSIRS/MSRIR and five times for MSIRN/MSIRNR), such that, for an MSIR model, the population, *n*, at time *t* was given by:

$$n(t) = (M_{1,t}, , \ldots M_{20,t}, S_{1,t}, \ldots S_{20,t}, I_{1,t}, \ldots I_{20,t}, R_{1,t}, \ldots R_{20,t})$$

After Metcalf et al., 2012, we next constructed a general transition matrix to project the population forward based on biweekly timesteps, chosen to roughly recapitulate the generation time for henipa- and filovirus infections (Hayman, 2015; Paweska et al., 2012; Swanepoel et al., 1996). When fully specified, the population transition matrix represented the product of demographic and epidemiological transitions, which varied based on the form

of the model being fit. Epidemiological transitions within each age class (a) could take on one of the two following forms:

(1) For an MSIR/MSRIR/MSIRS model:

$$\mathbf{A_{a,t}} = \begin{bmatrix} 1-\omega & 0 & 0 & 0 \\ \omega & 1-\lambda_t-\phi_t & 0 & \sigma \\ 0 & \lambda_t & 1-r & 0 \\ 0 & \phi_t & r & 1-\sigma \end{bmatrix}$$

(2) For an MSIRN/MSIRNR model:

$$\mathbf{A_{a,t}} = \begin{bmatrix} 1-\omega & 0 & 0 & 0 & 0 \\ \omega & 1-\lambda_t & 0 & 0 & 0 \\ 0 & \lambda_t & 1-r & 0 & 0 \\ 0 & 0 & r & 1-\sigma & \Gamma_t \\ 0 & 0 & 0 & \sigma & 1-\Gamma_t \end{bmatrix}$$

In the above transition matrices, ω represents the rate of waning immunity, λ_t the time-dependent "force of infection" (the rate at which susceptibles become infectious), ϕ_t the time-dependent "force of seroconversion," r the rate of recovery from infection (fixed at 1 biweek^{-1} for all model fits), σ the rate of antibody waning in adult-age individuals, and Γ_t the time-dependent "force of boosting."

$\lambda_t, \phi_t, \Gamma_t$ can be further defined as:

$$\lambda_t = 1 - exp(-\beta \frac{\sum I_t}{n_t})$$

460 *(3)*

$$\phi_t = 1 - exp(-\rho \frac{\sum I_t}{n_t})$$

461 *(4)*

$$\Gamma_t = 1 - exp(-\gamma \frac{\sum I_t}{n_t})$$

462 *(5)*

463 where β is the raw transmission coefficient, ρ the rate of dead-end seroconversion, and γ the

464 rate of antibody boosting, based on contact with infectious (I) individuals. In all cases, $\frac{\sum I_t}{n_t}$ is

465 the proportion of infectious individuals in the population at a given time.

466 Again following Metcalf et al., 2012, we project the entire population forward in

467 time, via aging, mortality and infection dynamics according to:

$$\mathbf{A(n(t))} = \begin{pmatrix} s_1(1-u_1)A_1 & 0 & 0 & \dots & 0 \\ s_1u_1A_1 & s_2(1-u_2)A_2 & 0 & \dots & 0 \\ 0 & s_2u_2A_2 & s_3(1-u_3)A_3 & \dots & 0 \\ 0 & 0 & s_3u_3A_3 & \dots & 0 \\ \dots & \dots & \dots & \dots & 0 \\ 0 & 0 & 0 & \dots & s_zA_z \end{pmatrix}$$

468 *(6)*

469 where s_a gives the age- and species-specific survival rate for the timestep of the model

470 (biweeks) and u_a gives the rate of aging out of age class a. A_1, A_2, A_3, etc. are defined in

471 equations (1) and (2) above. After each survival-epidemic transition, populations were

472 further subject to a reproductive transition, by which all adult bats in the second class of life

473 or higher reproduced by a fecundity rate (.48) multiplied by their age-specific survival rate

474 (s). Because our model tracked specific biweeks of the year (beginning with the species-

specific birth pulse as biweek one: October 1 for *P. rufus* and November 1 for *E. dupreanum*), we were able to normally distribute annual births within five biweeks on either side of the pulse. No reproduction was permitted throughout the rest of the year.

Natural mortality and epidemic transitions were allowed within each biweekly timestep, such that there were 26 opportunities for individuals to move between epidemic states within a given year. In all model runs, we initiated the population as almost entirely susceptible but introduced five infectious individuals in the third age cohort, then iterated forward until the population reached equilibrium (Fig. S13). To estimate epidemic parameters, we extracted one equilibrium year of model output, then minimized the negative log-likelihood of that model's fit to our age- and biweek-structured data for our longitudinally re-sampled Moramanga sites (Fig. S8, S9). We repeated all model fits and parameter estimates using data generated via the lower and upper threshold for seropositivity. In most cases, optimization was conducted using the "Nelder-Mead" algorithm in the optim() function of R, though in six cases (*E. dupreanum*: MSIRN-matSus-lci, MSIRNR-matAB-lci, MSIRNR-matSus-lci, MSIRNR-matAB-uci*; P. rufus*: MSIR-uci, MSIRN-matSus -uci), convergence errors forced us to adopt the 'BFGS' algorithm instead.

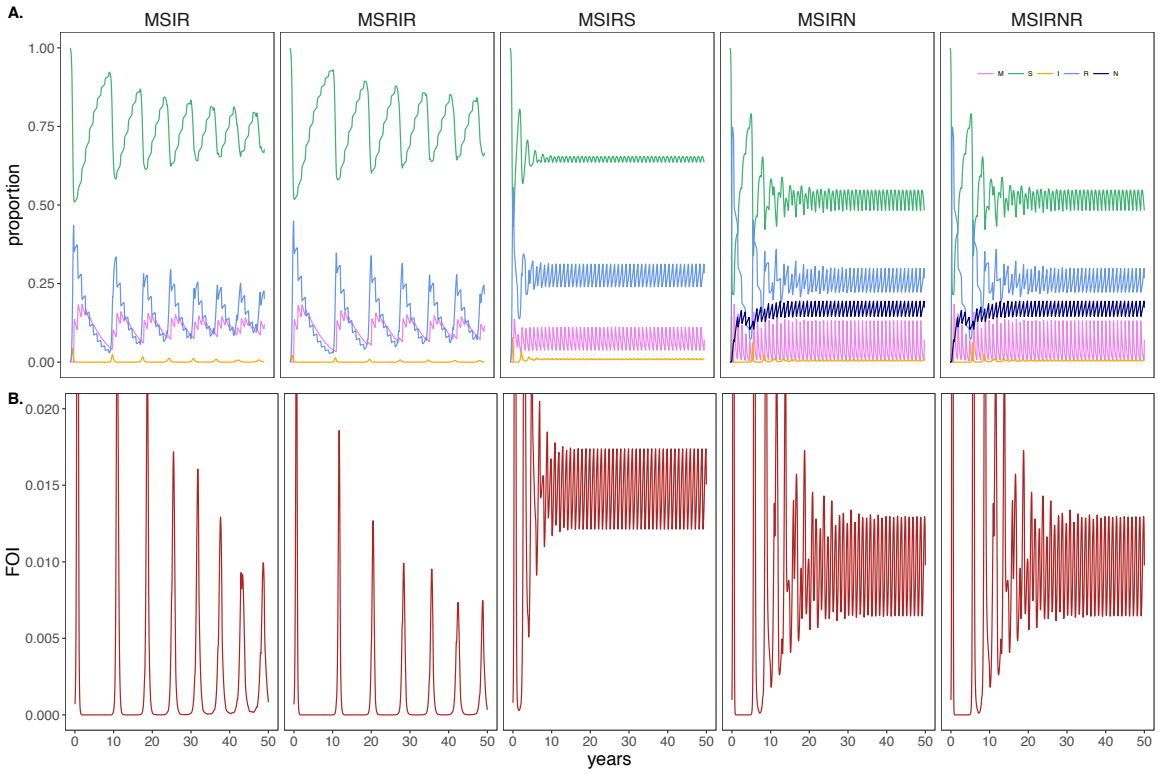

Fig. S13. ***Fifty year model time series***
Upper panels **(A)** given the time series of population state proportions across the first fifty years of model runs for all five tested models (MSIR, MSRIR, MSIRS, MSIRN, and MSRINR; note that MSIRN/R runs shown here are for matAB assumptions of inherited maternal immunity). In all cases, the time series was run using parameters fit to the *E. dupreanum* upper MFI cutoff for seropositivity (Table S7). Our matrix models tracked individuals within twenty age classes across each of the colored epidemic states shown (ages are summed within disease state for the purposes of this plotting). Total population size was held constant at 10000 individuals, and a stable age structure was maintained across this time series. We fit the age- and seasonally-structured model seroprevalence from the last year of each time series at equilibrium to our corresponding data. **(B)** Force of infection (FOI, λ), or the rate at which susceptibles (S) become infectious (I), over time, for the 50-year simulation, by model type. FOI is the product of the transmission coefficient (ß) and the proportion of the infectious population at a given timepoint. FOI thus cycled annually in our model runs, oscillating around an equilibrium with the infectious population.

We extracted the Hessian matrix from each model fit to generate 95% confidence intervals for each estimated parameter and the corresponding seroprevalence generated by the model. We report all estimated parameter values, confidence intervals, and raw AIC scores for each fitted model in Table S7. For MSIR models, we estimated only two parameters, the rate of waning maternal immunity (ω) and the transmission coefficient (β).

For MSIRS and MSIRN models, we estimated ω, β, plus the rate waning humoral immunity (σ). For MSRIR models, we estimated ω, β, plus the direct rate of seroconversion from S to R based on contact with the infectious population (ρ). For MSIRNR models, we estimated ω, β, σ, and the rate of antibody boosting given contact between N- and I-class individuals (γ). The least parsimonious MSIRNR model was subsequently the most heavily penalized in tabulations of AIC.

Table S7. Model comparison and parameter estimation

Species	Antigen	MFI cutoff	Model†	AIC	k††	neg log-lik	Fitted par (mean [lci, uci])				
							ω	β	σ	ρ	γ
		mean	MSIR	95.2	2	45.58	0.2 [0-0.55]	1.39 [1.32-1.47]	0 [0-0]	0 [0-0]	0 [0-0]
			MSIRN-matAB	**93.3**	**3**	**43.67**	**0.12 [0-1.71]**	**1.96 [1.67-2.24]**	**0.01 [0-1.02]**	**0 [0-0]**	**0 [0-0]**
			MSIRN-matSus	94.6	3	44.29	0.08 [0-2.41]	1.97 [1.69-2.26]	0.01 [0-1.04]	0 [0-0]	0 [0-0]
			MSIRNR-matAB	95.3	4	43.67	0.12 [0-1.71]	1.96 [1.67-2.24]	0.01 [0-1.03]	0 [0-0]	0 [0-56.73]
			MSIRNR-matSus	96.9	4	44.46	0.05 [0.03-0.06]	2.25 [2.24-2.26]	0.01 [0-0.08]	0 [0-0]	1.29 [1.19-1.38]
			MSIRS	93.9	3	43.93	1.09 [0.53-1.65]	1.58 [1.4-1.76]	0.02 [0-2.3]	0 [0-0]	0 [0-0]
			MSRIR	96.8	3	45.38	0.19 [0-0.42]	1.36 [1.27-1.46]	0 [0-0]	1.23 [0.75-1.72]	0 [0-0]
E. dupreanum	NiV-G	lci	MSIR	102.3	2	49.13	0.2 [0-0.49]	1.5 [1.3-1.69]	0 [0-0]	0 [0-0]	0 [0-0]
			MSIRS	102.1	3	48.03	1.74 [0-4.61]	1.77 [1.52-2.02]	0.06 [0-1.44]	0 [0-0]	0 [0-0]
			MSRIR	103.9	3	48.94	0.22 [0-0.65]	1.44 [1.33-1.55]	0 [0-0]	1.42 [0-4.49]	0 [0-0]
			MSIRN-matAB	**100.1**	**3**	**47.04**	**0.09 [0.08-0.1]**	**2.31 [2.3-2.32]**	**0.01 [0-0.85]**	**0 [0-0]**	**0 [0-0]**
			MSIRN-matSus*	100.9	3	47.44	0.07 [0-0.75]	2.49 [2.49-2.49]	0.01 [0-1]	0 [0-0]	0 [0-0]
			MSIRNR-matAB*	102.1	4	47.05	0.09 [0.07-0.1]	2.31 [2.29-2.32]	0.01 [0-1.11]	0 [0-0]	0.03 [0-42.85]
			MSIRNR-matSus*	103.4	4	47.68	0.05 [0-0.12]	2.32 [2.32-2.33]	0.01 [0-0.09]	0 [0-0]	0.6 [0.52-0.68]
		uci	MSIR	56.1	2	26.07	0.2 [0-1.35]	1.13 [1.08-1.19]	0 [0-0]	0 [0-0]	0 [0-0]
			MSIRS	53.2	3	23.6	0.58 [0.13-1.03]	1.4 [1.39-1.41]	2.09 [2.09-2.09]	0 [0-0]	0 [0-0]
			MSRIR	65.1	3	29.53	0.2 [0.2-0.2]	1.59 [1.59-1.59]	0 [0-0]	1.62 [1.62-1.62]	0 [0-0]
			MSIRN-matAB	**52.3**	**3**	**23.16**	**0.29 [0-2.04]**	**1.97 [1.14-2.8]**	**0.07 [0-1.52]**	**0 [0-0]**	**0 [0-0]**
			MSIRN-matSus	55.2	3	24.61	0.03 [0-2.33]	1.74 [1.56-1.92]	0.04 [0-1.04]	0 [0-0]	0 [0-0]
			MSIRNR-matAB*	54.3	4	23.16	0.29 [0-2.04]	1.97 [1.14-2.8]	0.07 [0-1.51]	0 [0-0]	0 [0-35.28]
			MSIRNR-matSus	56.6	4	24.28	0.03 [0.03-0.04]	2.27 [2.27-2.27]	0.08 [0.08-0.08]	0 [0-0]	0.78 [0.72-0.85]
P. rufus	EBOV-Gp	mean	MSIR	92.1	2	44.05	0.24 [0-1.56]	1.15 [1.1-1.19]	0 [0-0]	0 [0-0]	0 [0-0]

	MSIRS	92.9	3	43.47	1.42 [0.2-2.63]	1.2 [1.1-1.29]	0.18 [0-1.29]	0 [0-0]	0 [0-0]
	MSRIR	94.1	3	44.05	0.24 [0-1.56]	1.15 [1.1-1.19]	0 [0-0]	0 [0-84.33]	0 [0-0]
	MSIRN-matAB	**88.7**	**3**	**41.36**	**0.47 [0-1.23]**	**1.97 [1.86-2.08]**	**0.05 [0-0.75]**	**0 [0-0]**	**0 [0-0]**
	MSIRN-matSus	90.5	3	42.26	0.24 [0-2.56]	2.02 [1.71-2.32]	0.05 [0-0.69]	0 [0-0]	0 [0-0]
	MSIRNR-matAB	90.7	4	41.36	0.47 [0-1.23]	1.97 [1.86-2.08]	0.05 [0-0.75]	0 [0-0]	0.01 [0-29.16]
	MSIRNR-matSus	92.5	4	42.26	0.24 [0-2.56]	2.02 [1.72-2.32]	0.05 [0-0.69]	0 [0-0]	0 [0-41.27]
lci	MSIR	107.1	2	51.54	0.18 [0-0.99]	1.19 [1.06-1.32]	0 [0-0]	0 [0-0]	0 [0-0]
	MSIRS	108	3	50.97	1.72 [1.64-1.8]	1.24 [1.14-1.34]	0.12 [0-0.69]	0 [0-0]	0 [0-0]
	MSRIR	109.1	3	51.53	0.2 [0-2.44]	1.19 [1.03-1.34]	0 [0-0]	1.1 [0-29.97]	0 [0-0]
	MSIRN-matAB	**102.4**	**3**	**48.21**	**0.37 [0-1.06]**	**1.95 [1.89-2.02]**	**0.04 [0-0.77]**	**0 [0-0]**	**0 [0-0]**
	MSIRN-matSus	106.9	3	50.47	0.18 [0-1.96]	1.88 [1.73-2.03]	0.03 [0-0.8]	0 [0-0]	0 [0-0]
	MSIRNR-matAB	104.4	4	48.21	0.37 [0-1.06]	1.95 [1.89-2.02]	0.04 [0-0.77]	0 [0-0]	0 [0-159.98]
	MSIRNR-matSus	108.1	4	50.03	0.2 [0-1.92]	1.96 [1.78-2.14]	0.04 [0-2.47]	0 [0-0]	1.05 [0-13.32]
uci	MSIR*	45.4	2	20.69	0 [0-48.54]	1.07 [1.03-1.12]	0 [0-0]	0 [0-0]	0 [0-0]
	MSIRS	46.3	3	20.16	1.4 [1.4-1.4]	1.08 [1.07-1.09]	0.37 [0.35-0.38]	0 [0-0]	0 [0-0]
	MSRIR	47.3	3	20.65	0 [0-290.05]	1.14 [0.96-1.31]	0 [0-0]	24.7 [21.39-28.01]	0 [0-0]
	MSIRN-matAB	**45.4**	**3**	**19.68**	**1.92 [1.04-2.8]**	**1.91 [1.8-2.02]**	**0.13 [0-1.23]**	**0 [0-0]**	**0 [0-0]**
	MSIRN-matSus*	46.9	3	20.46	0 [0-101.85]	1.17 [1.02-1.33]	0.06 [0-1.97]	0 [0-0]	0 [0-0]
	MSIRNR-matAB	47.4	4	19.68	1.92 [1.04-2.8]	1.91 [1.8-2.02]	0.13 [0-1.23]	0 [0-0]	0 [0-186.26]
	MSIRNR-matSus	47.5	4	19.73	1.88 [0-5.15]	1.9 [1.7-2.09]	0.13 [0-1.17]	0 [0-0]	0 [0-242.85]

Best-fit models for each data subset are highlighted in **bold** (always MSIRN-matAB).

*These models (*E. dupreanum*: MSIRN-matSus-lci, MSIRNR-matAB-lci, MSIRNR-matSus-lci, MSIRNR-matAB-uci; *P. rufus*: MSIR-uci, MSIRN-matSus -uci) were fit using the "BFGS" method in the optim() function of R. All other fits used the "Nelder-Mead" method.

†For all MSIRN and MSIRNR models fit, we explored both scenarios in which N-class dams produced S- and M-class pups. In all cases, "-matSus" indicates a form of the model in which N-class dams gave birth to susceptible (S) pups and "-matAB" indicates a form of the model in which N-class dams gave birth to maternally immune (M) pups

††The parameter *k* indicates the number of parameters fit for each model type.

537
538

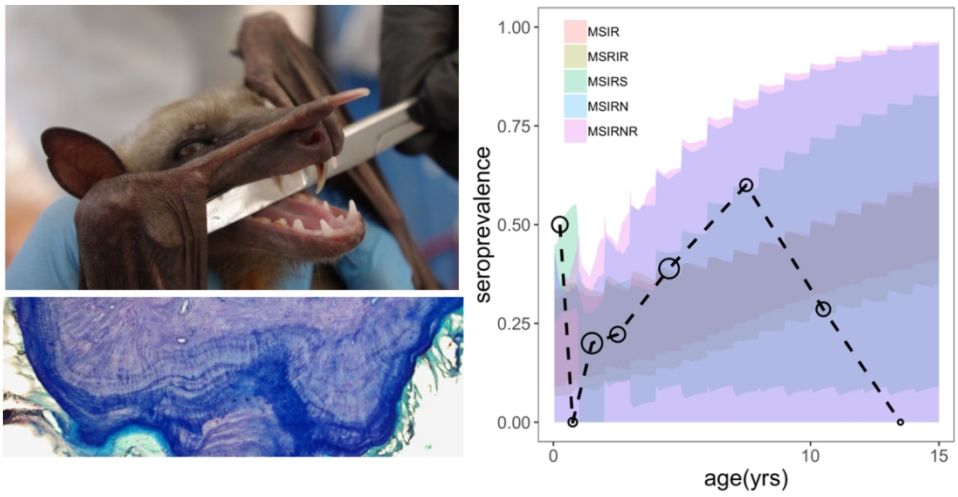

The authors contructed age-seroprevalence curves for henipa- and filoviruses in Madagascar fruit bats and fit a suite of mechanistic transmission models to the resulting data. Here, we show the Madagascan fruit bat (Eidolon dupreanum), with cementum annuli from teeth in cross section. The age-seroprevalence curve for anti-NiV-G antibodies in E. dupreanum is shown in conjunction with fits via multiple transmission models.

109x55mm (300 x 300 DPI)